Effects of LH and ICRF power on SOL density profiles and LH coupling on the Alcator C-Mod tokamak

C. Lau[1], G.R Hanson[2], Y. Lin[1], J. Wilgen[2], S. Wukitch[1], G. Wallace[1] and the Alcator C-Mod team

[1] MIT Plasma Science and Fusion Center

[2] Oak Ridge National Laboratory

ORNL FEST Seminar 3/26/2013

Table of Contents

- Why we study RF-SOL interactions and RF coupling?
- X-mode scrape-off layer (SOL) reflectometer density profile measurement
- Effects of lower hybrid (LH) power on SOL density profiles and LH coupling
- Effects of LH+ ion cyclotron range of frequencies (ICRF) power on SOL density profiles and LH coupling

Why we study RF-SOL interactions and RF coupling?

- ICRF and LH are used to heat and drive current in tokamak plasmas

- RF-SOL interactions are undesirable
  - RF plasma-antenna coupling, ICRF sheaths, SOL absorption

- Radial and poloidal density profile is an important and rarely measured parameter that affects RF physics
  - cold wave theory depends on density and magnetic field
  - LH slow wave and ICRF fast wave are evanescent below cutoff density of 2.6×10^{17} m^{-3} and ~ 5×10^{18} m^{-3}
  - Density gradients are also important
  - ICRF sheath rectification[1] is strongly dependent on density (and temperature)

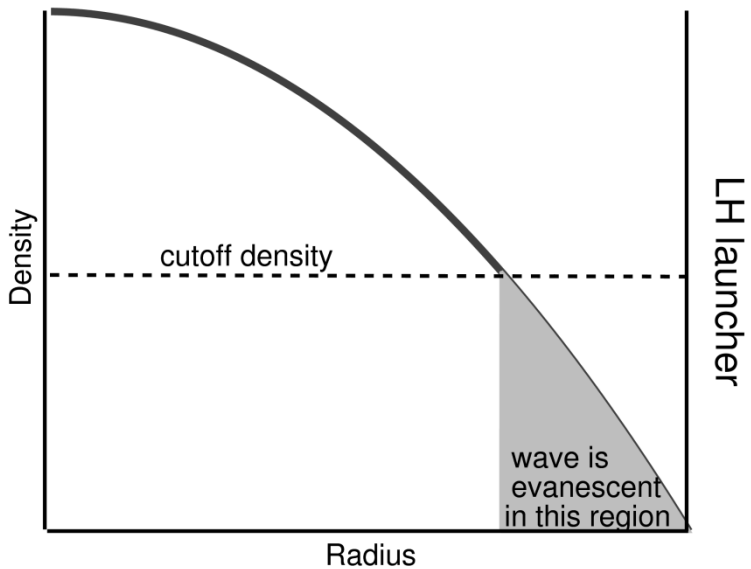

[1]Myra, PRL 2008

SOL can affect ICRF and LH physics, but ICRF and LH power also modifies SOL parameters

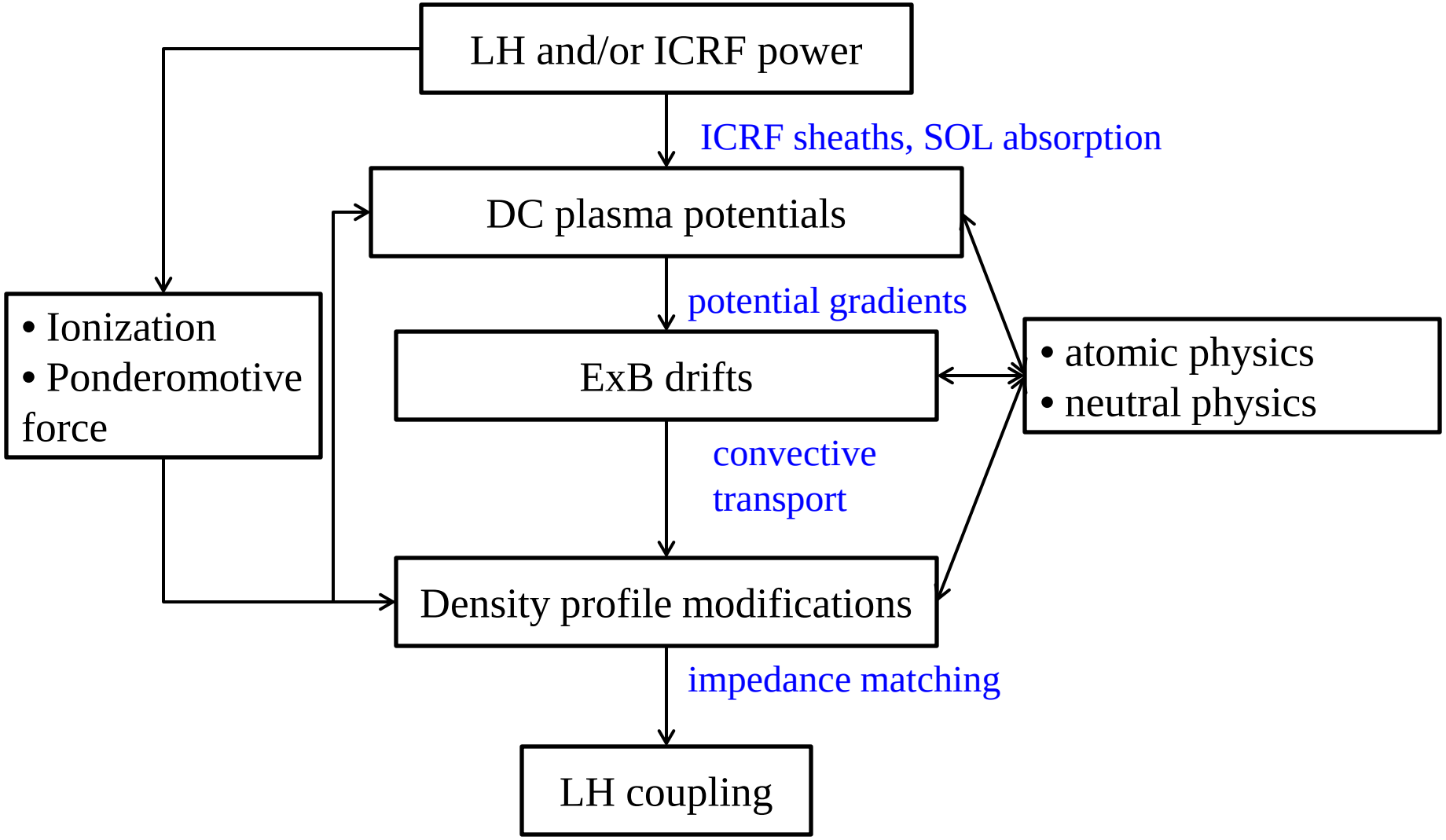

Understanding how ICRF and LH power modifies SOL density profile and RF coupling is main purpose of this thesis

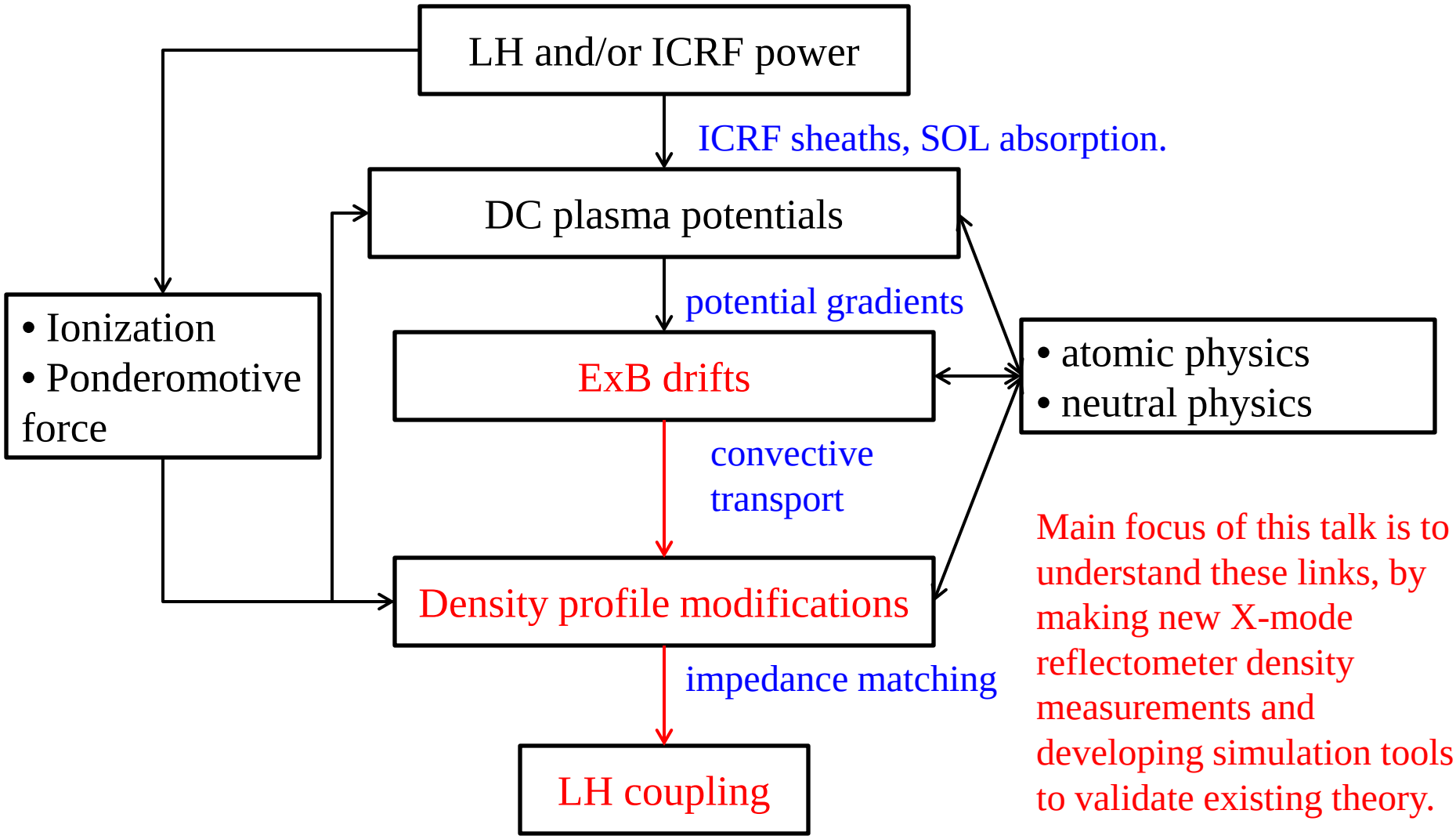

Main focus of this talk is to understand these links, by making new X-mode reflectometer density measurements and developing simulation tools to validate existing theory.

Table of Contents

- Why we study RF-SOL interactions and LH coupling?
- X-mode SOL reflectometer density profile measurement
- Effects of LH power on SOL density profiles and LH coupling
- Effects of LH+ICRF power on SOL density profiles and LH coupling

Reflectometry density profile measurement

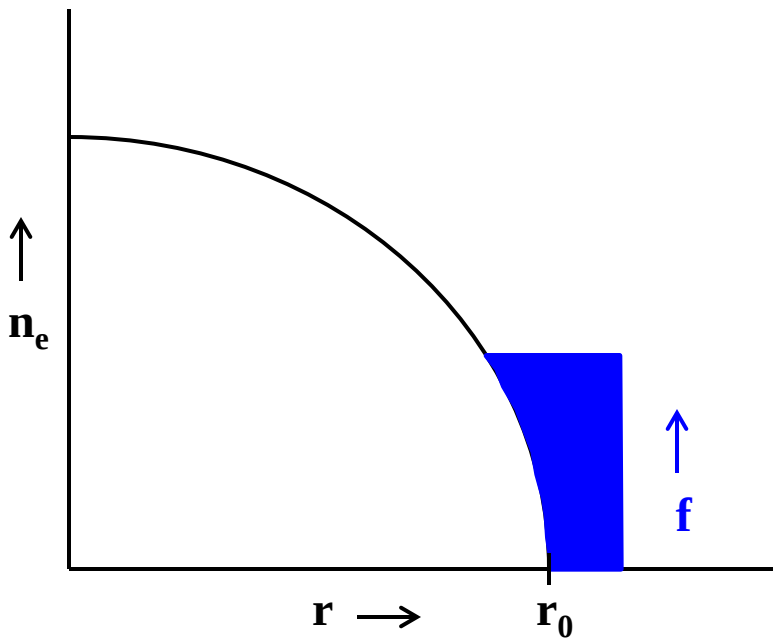

Sweeping frequency, f, is used to get profile information

$$\phi(f) = 4\pi \frac{f}{c} \int_{r0}^{r(f)} N(n(r,f), B(r,f))dr - \pi/2$$

where *N* is the index of refraction of the X-mode R cutoff, ϕ is the phase, and r is the radial location of cutoff layer

• design, implementation, and analysis challenges of new X-mode SOL reflectometer diagnostic

SOL reflectometer electronics on Alcator C-Mod

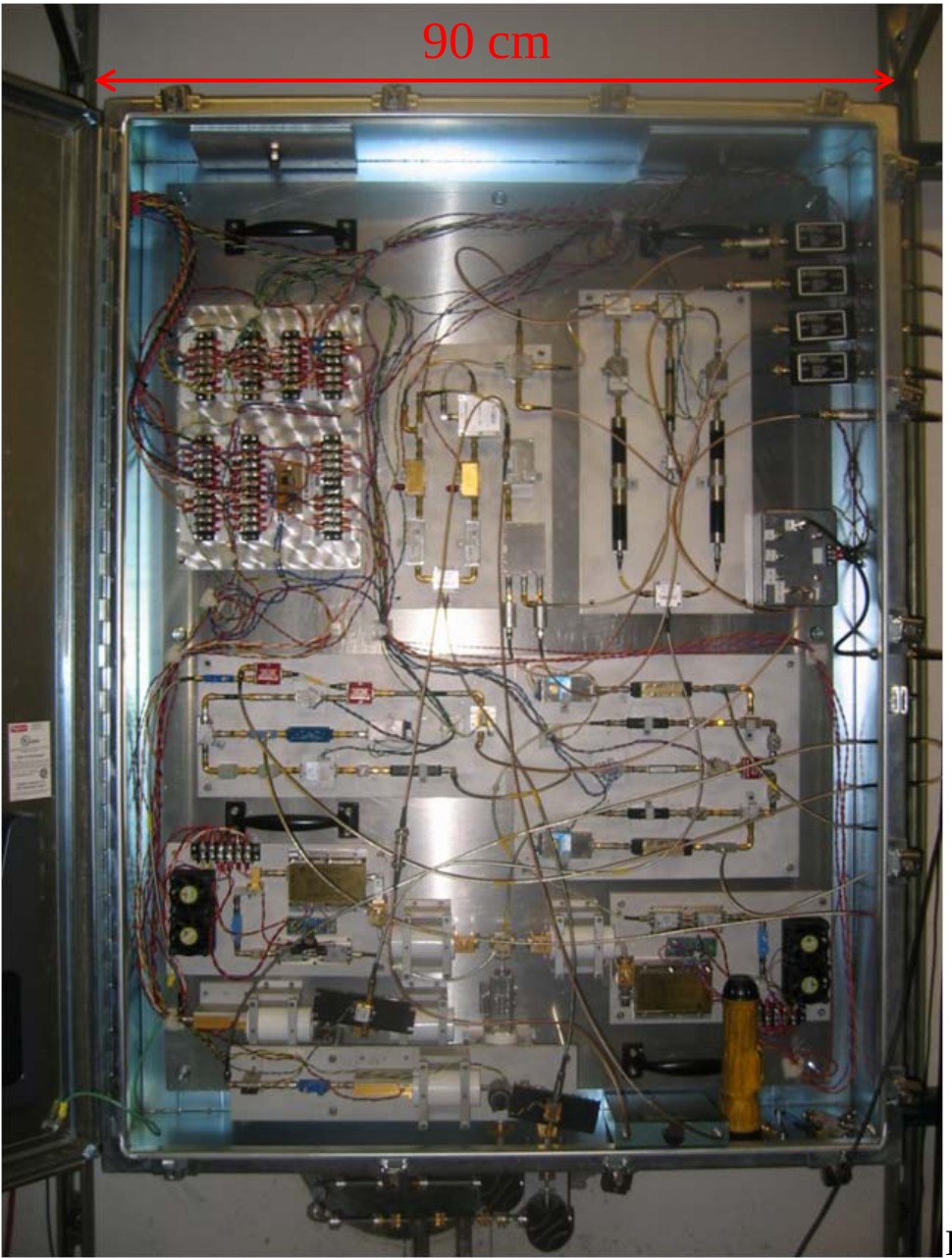

- use X-mode R-cutoff frequency range from 100-146 GHz
  - yields density range of $5x10^{16}$ to ~$5x10^{19}$ m^{-3} at B_0= 5.4T
  - 40μs time resolution
- Source frequency is VCO (6.3-9.2 GHz)
- Frequency multipliers, mixers, filters etc. are used to achieve 100-146 GHz source frequency
  - considerable work to reduce spurious harmonics and maximize signal levels
- Heterodyne detection circuit
  - 1.7GHz I (Acosϕ) and Q (Asinϕ) detectors

Hanson et al, RSI 2008 C Lau et al, RSI 2012

SOL reflectometer transmission line

- Transmission line uses fundamental (TE_{10}) WR-08 (2 mm x 1 mm), tallguide (TE_{01}) WR-22, and tallguide WR-90 waveguides to reduce transmission line loss
  - expected resistive loss for WR-08, WR-22, WR-90 is 8, 1.6, and .2 dB/m
  - mode conversion is calculated by 3D FEM simulations in COMSOL
  - significant number of tapers, bends, and twists need to be designed due to space constraints
  - estimated 27dB total loss

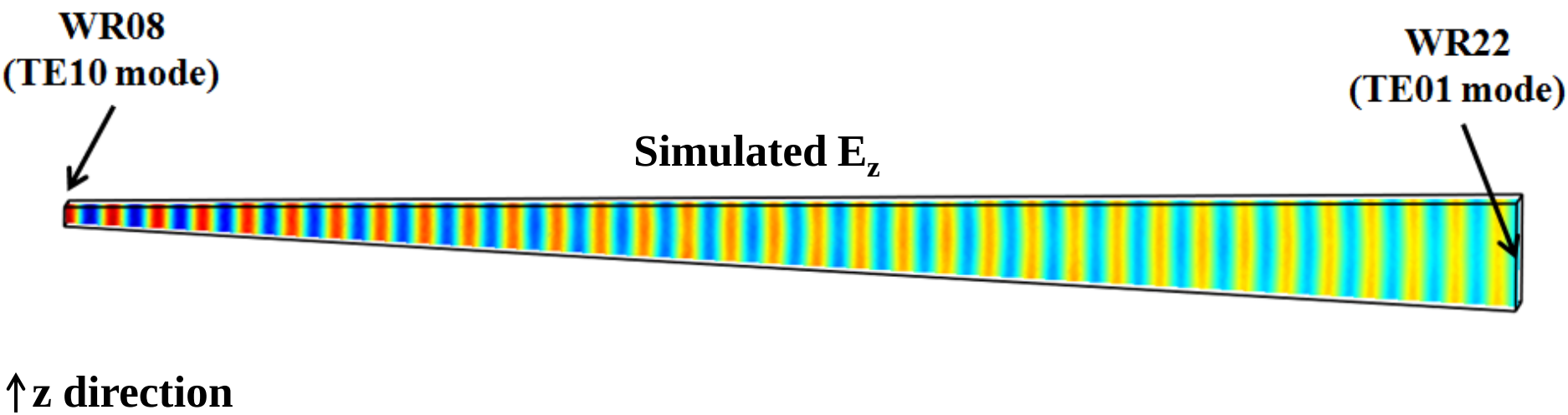

SOL reflectometer transmission line

- Transmission line uses fundamental (TE_{10}) WR-08 (2 mm x 1 mm), tallguide (TE_{01}) WR-22, and tallguide WR-90 waveguides to reduce transmission line loss
  - expected resistive loss for WR-08, WR-22, WR-90 is 8, 1.6, and .2 dB/m
  - mode conversion is calculated by 3D FEM simulations in COMSOL
  - significant number of tapers, bends, and twists need to be designed due to space constraints
  - estimated 27dB total loss
- WR-22 waveguides are shown adjacent to LH launcher
  - constant radius of curvature bends
  - hyperbolic secant radius of curvature bends, so that horn is perpendicular to flux surface

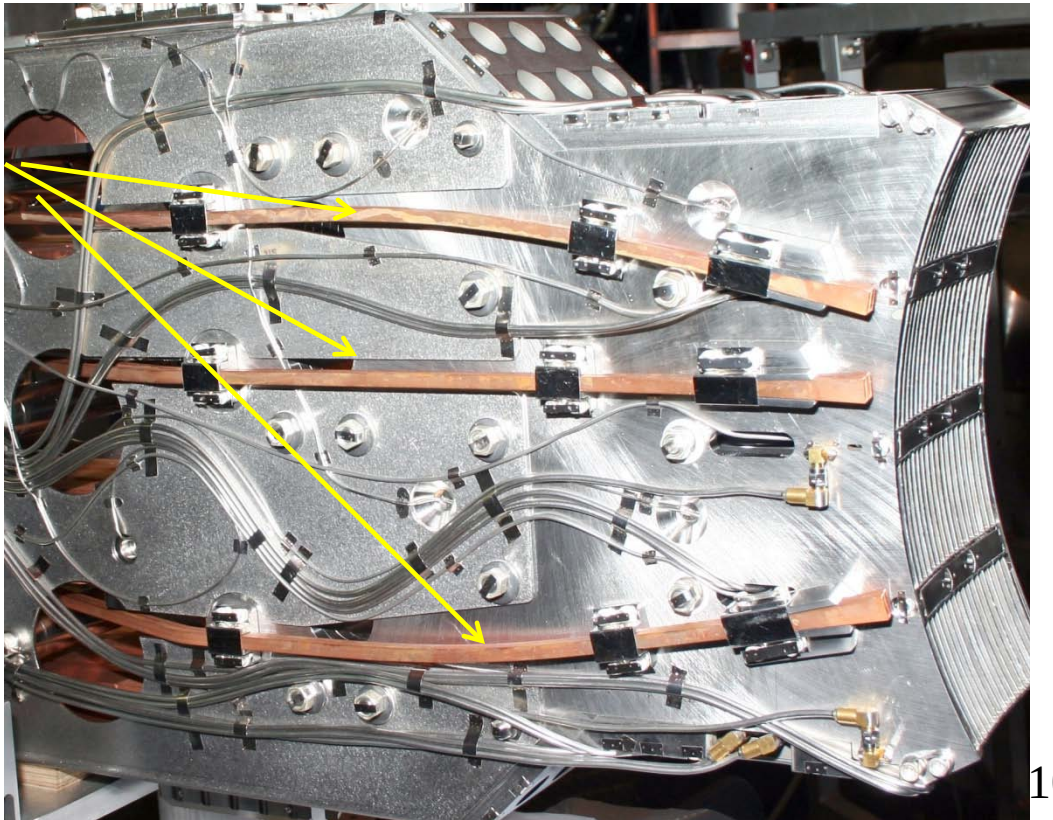

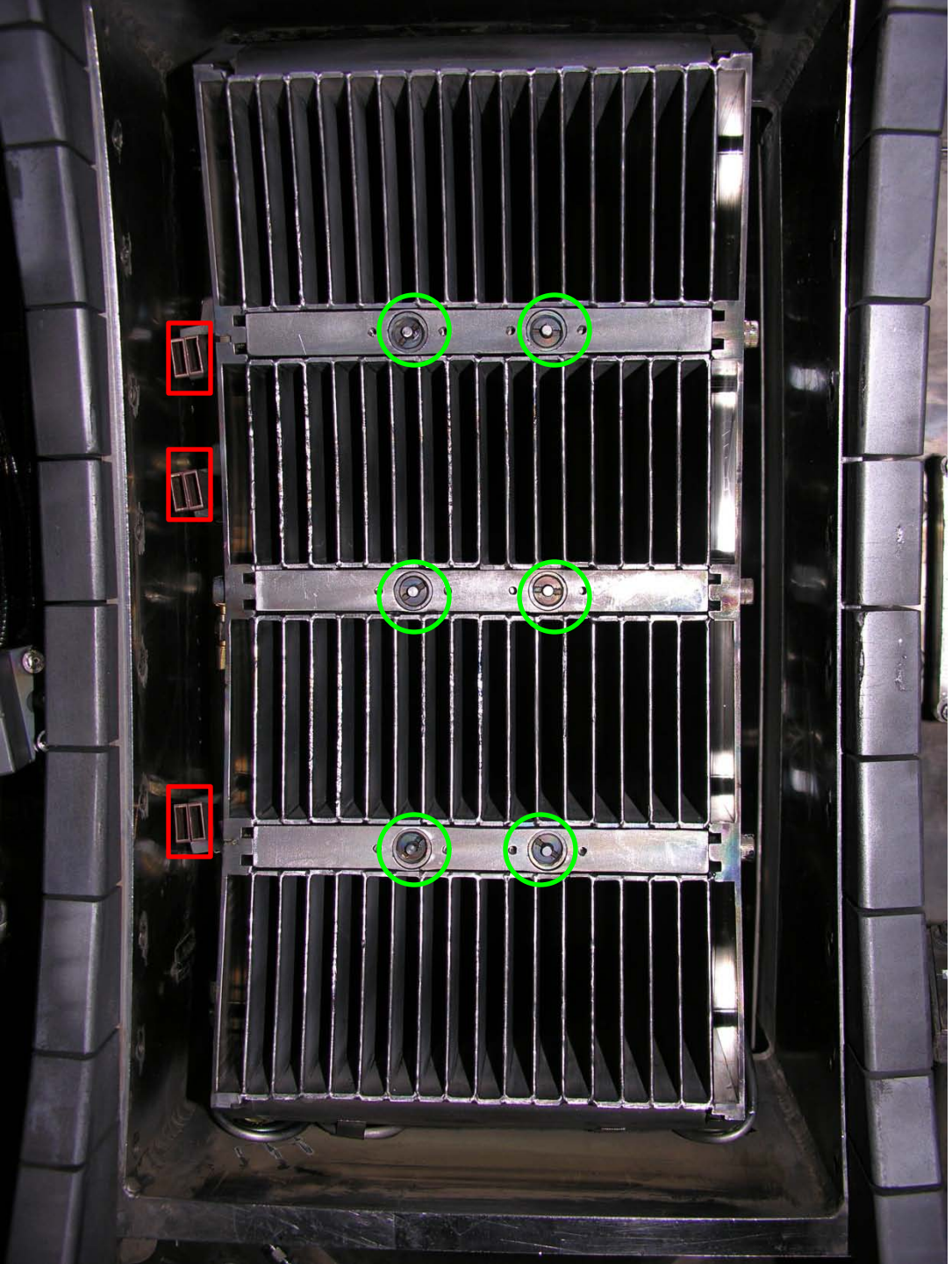

LH-SOL Reflectometer

- measurement at 3 pairs of reflectometer horns
- 10° twist to tilt reflectometer horn to preferentially launch and receive X-mode
- only one set of electronics, so waveguide switch is used to select location for each discharge
- 6 Langmuir probes each used to measure density and temperature at one location

LH-SOL Reflectometer

Cartoon of desired single reflection versus spurious double reflection signals

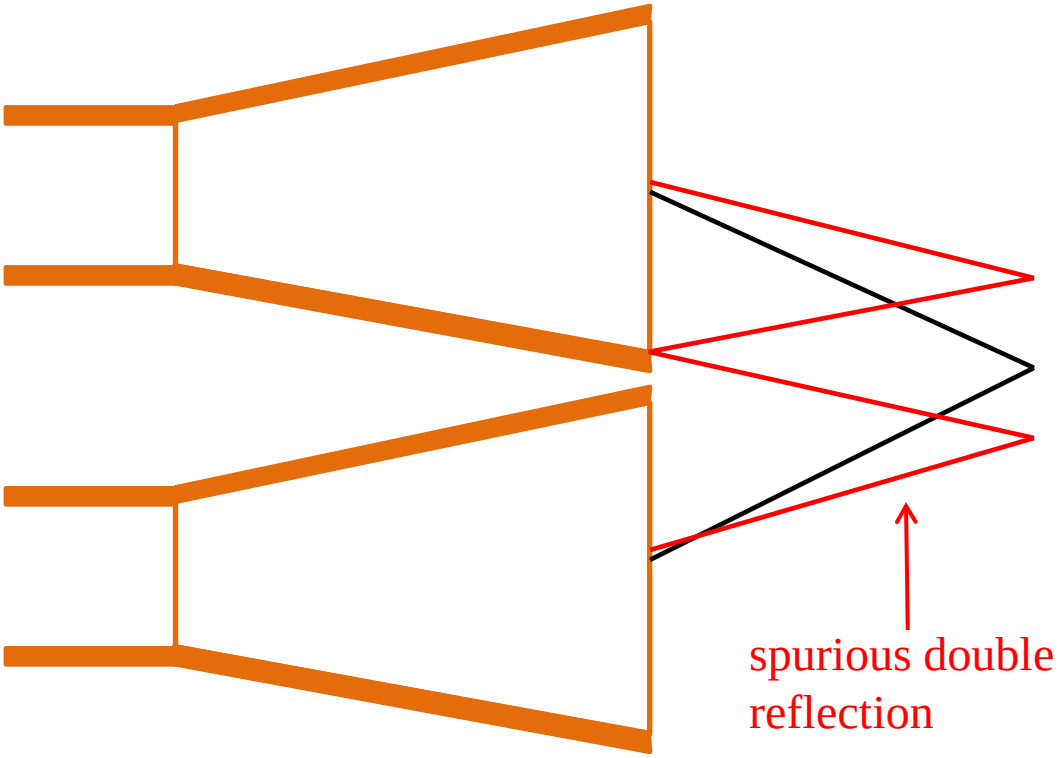

horn to horn coupling loss is 19dB

- measurement at 3 pairs of reflectometer horns
- 10° twist to tilt reflectometer horn to preferentially launch and receive X-mode
- only one set of electronics, so waveguide switch is used to select location for each discharge
- 6 Langmuir probes each used to measure density and temperature at one location
- 3D FEM simulations indicate effect of spurious reflections need to be minimized

Reflectometer phase measurement analysis

- Measured signal is I [A cos(φ(t))] and Q [A sin(φ(t))] where φ is the phase
  - Peak fourier frequency of scalogram of I+ iQ is given by dφ/dt
  - Scalogram provides temporal and fourier frequency filtering to reduce, but not eliminate, effects of density fluctuations on the density measurement

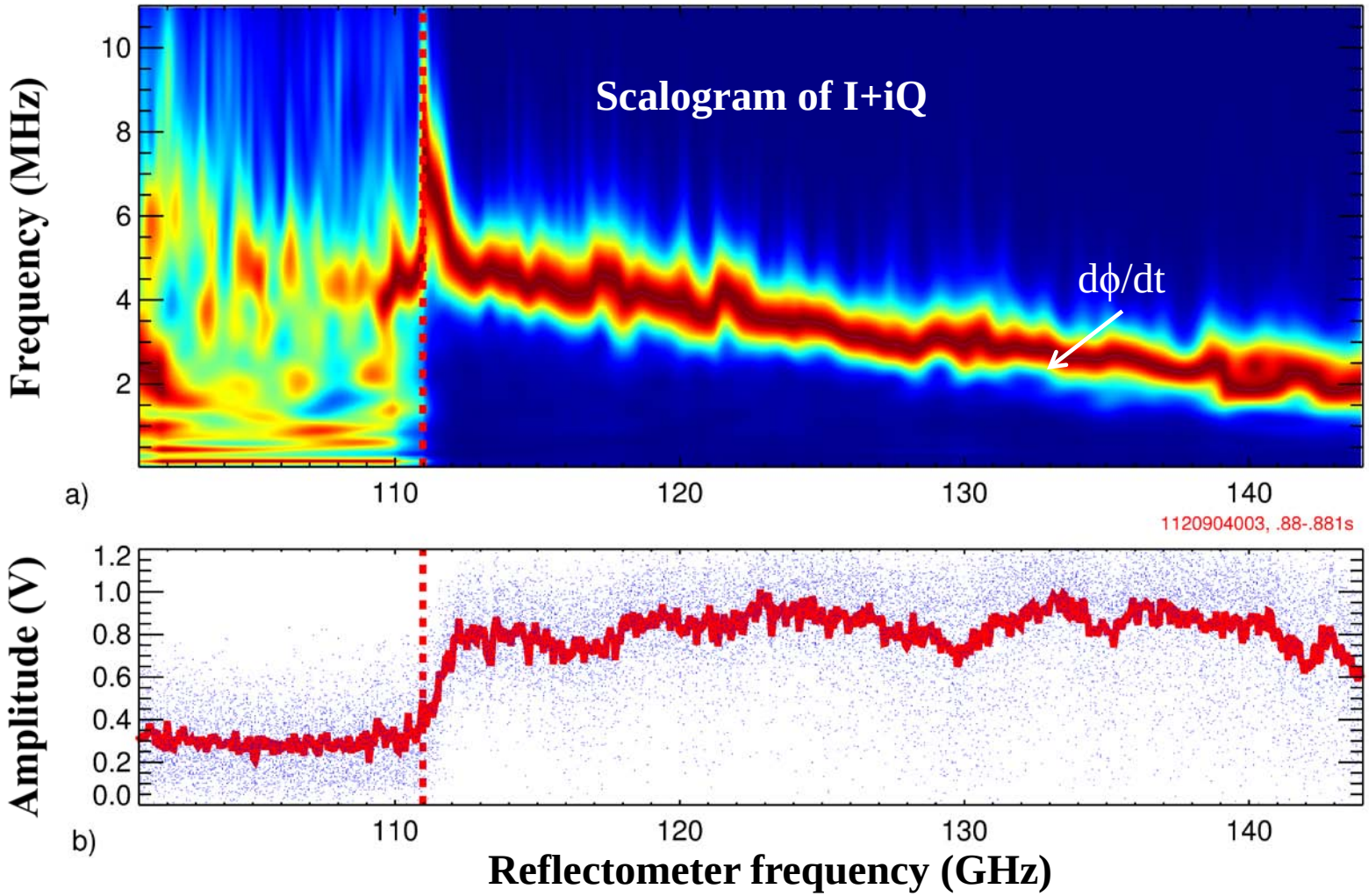

Density profile can be determined by phase inversion

$$\phi(\omega) = 2\frac{\omega}{c}\int_{r_0}^{r(\omega)} N dr - \pi/2$$

Reflectometer equation

$$\boldsymbol{r}(\omega) = \boldsymbol{r}_0 - \frac{\boldsymbol{c}}{\pi}\int_0^{\omega} \frac{\boldsymbol{d}\phi}{\boldsymbol{d}\omega'} \frac{\boldsymbol{d}\omega'}{(\omega^2 - \omega'^2)^{1/2}}$$

O-Mode

$$\boldsymbol{r}(\omega_{\boldsymbol{i}+1}) = \boldsymbol{r}_0 - \boldsymbol{f}(\phi_{\boldsymbol{i}}, \phi_{\boldsymbol{i}-1}..., \omega_{\boldsymbol{i}}, \omega_{\boldsymbol{i}-1}..., \boldsymbol{r}(\omega_{\boldsymbol{i}}), \boldsymbol{r}(\omega_{\boldsymbol{i}-1})..., \boldsymbol{B}(\boldsymbol{r}))$$

X-mode[1]

[1]Bottolier-Curtet, RSI 1987

Radial errors in density profile inversion is dominant error source

$$\phi(\omega) = 2\frac{\omega}{c}\int_{r_0}^{r(\omega)} N dr - \pi/2$$

Reflectometer equation

$$\boldsymbol{r}(\omega) = \boldsymbol{r}_0 - \frac{\boldsymbol{c}}{\pi}\int_0^{\omega} \frac{\boldsymbol{d}\phi}{\boldsymbol{d}\omega'} \frac{\boldsymbol{d}\omega'}{(\omega^2 - \omega'^2)^{1/2}}$$

O-Mode

$$\boldsymbol{r}(\omega_{i+1}) = \boxed{\boldsymbol{r}_0} - \boldsymbol{f}(\phi_i, \phi_{i-1}..., \omega_i, \omega_{i-1}..., \boldsymbol{r}(\omega_i), \boldsymbol{r}(\omega_{i-1})..., \boldsymbol{B}(\boldsymbol{r}))$$

X-mode

- 0.1% error in |B| ~.7 mm error in r_0
- Calibration errors in B_t up to 1%
- Density profile is shifted to match closest Langmuir probe data during ohmic discharges
- Relative shift of first cutoff layer between OH and ICRF discharges can be used to constrain discharges with ICRF power
- ~ 1-3mm radial error

Ideal signal levels

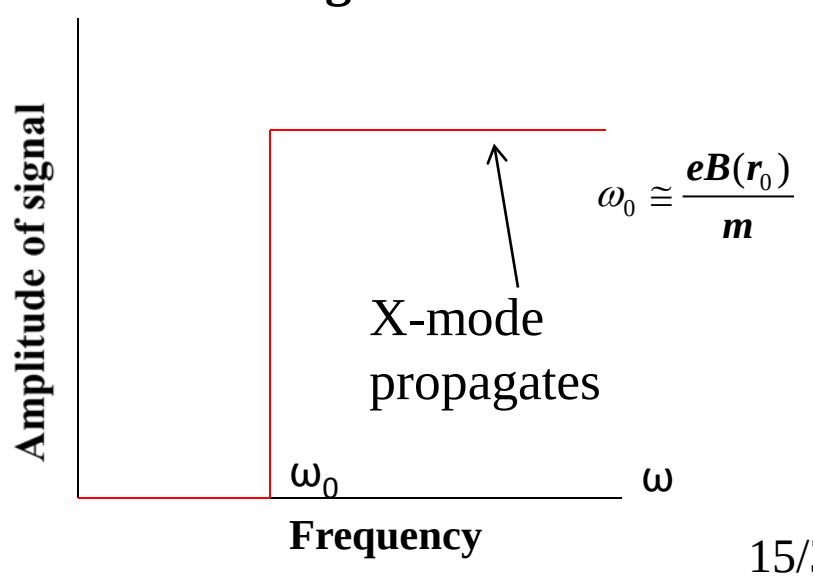

Phase errors are dominant contribution to density profile shape errors

$$\phi(\omega) = 2\frac{\omega}{c}\int_{r_0}^{r(\omega)} N dr - \pi/2$$

Reflectometer equation

$$\boldsymbol{r}(\omega) = \boldsymbol{r}_0 - \frac{\boldsymbol{c}}{\pi}\int_0^{\omega} \frac{\boldsymbol{d}\phi}{\boldsymbol{d}\omega'} \frac{\boldsymbol{d}\omega'}{(\omega^2 - \omega'^2)^{1/2}}$$

O-Mode

$$\boldsymbol{r}(\omega_{\boldsymbol{i}+1}) = \boldsymbol{r}_0 - \boxed{\boldsymbol{f}(\phi_{\boldsymbol{i}}, \phi_{\boldsymbol{i}-1}..., \omega_{\boldsymbol{i}}, \omega_{\boldsymbol{i}-1}..., \boldsymbol{r}(\omega_{\boldsymbol{i}}), \boldsymbol{r}(\omega_{\boldsymbol{i}-1})..., \boldsymbol{B}(\boldsymbol{r}))}$$

X-mode

- Largest contribution to f(…) is phase measurement
- Systematic phase errors (waveguide calibration etc.)
  - same error for all profiles, so systematic errors do not contribute to relative density profile shapes
- Statistical, inversion errors accounted for by error bars
  - density profile is inverted at 1 ms time resolution (25 phase measurements at 40μs time resolution are first averaged)
  - for steady state discharges, shaded error bars represent the ±1 standard deviation of the radial error of collection of averaged profiles over at least 50 ms

Comparison between scanning Langmuir probes and SOL reflectometer in ohmic discharges shows good agreement throughout SOL

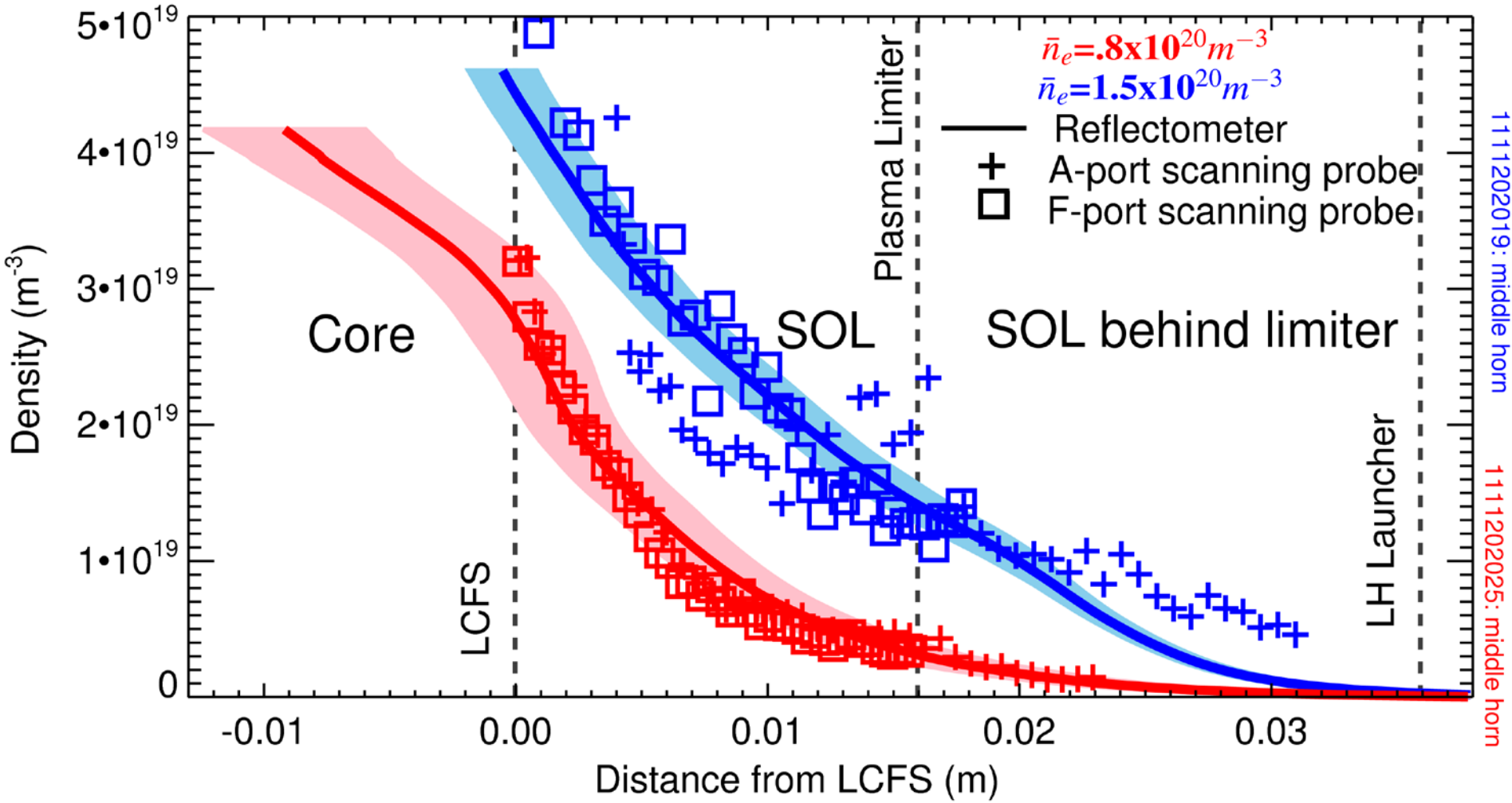

Note: reflectometers and scanning probes are at different toroidal locations

Table of Contents

- Why we study RF-SOL interactions and LH coupling?
- X-mode SOL reflectometer density profile measurement
- Effects of LH power on SOL density profiles and LH coupling
- Effects of LH+ICRF power on SOL density profiles and LH coupling

LH modifies density profile on *fast* timescale less than 1ms

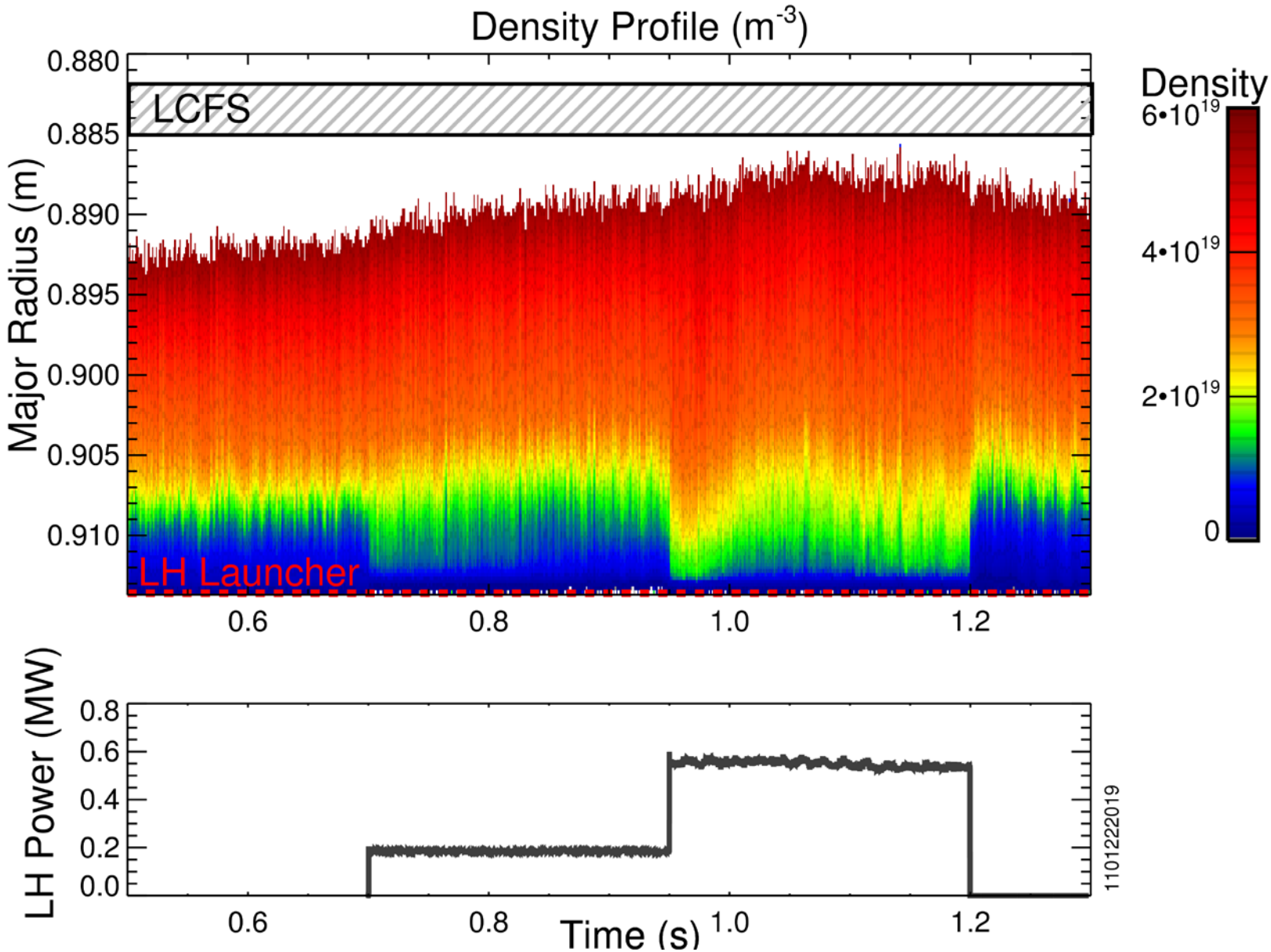

Reflectometer measures LH-induced poloidal density asymmetries, consistent with video camera images

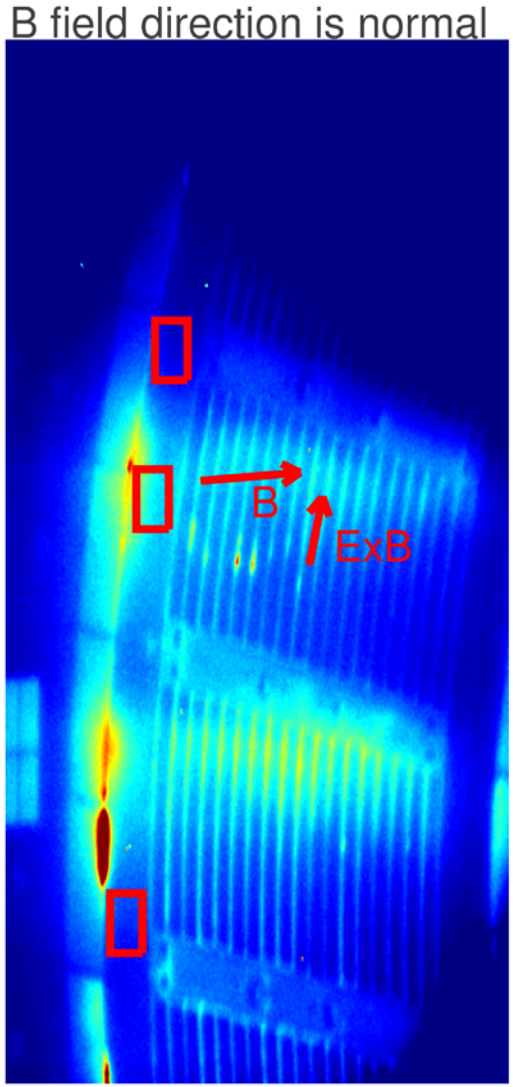

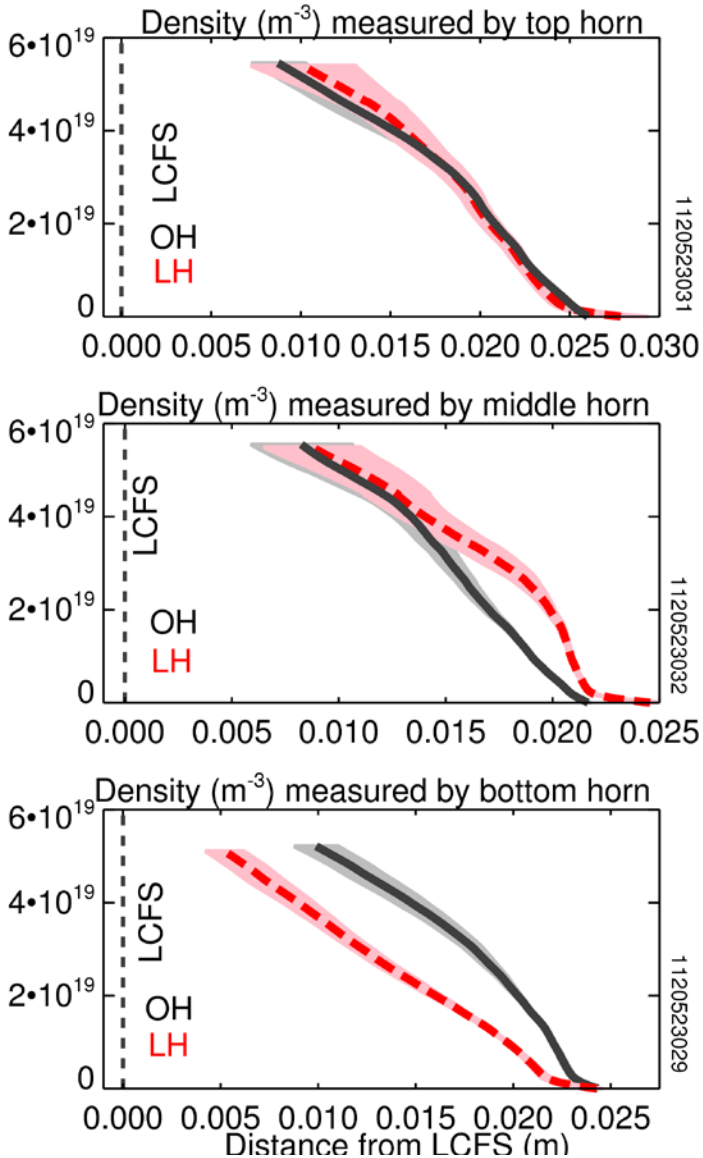

- LH power drives:
  - density modifications that correlate with emissivity striations
  - little to no modification at top horn
  - strong density increase at middle horn
  - strong density decrease at bottom horn

$\bar{n}_e$ =1.6x10^{20} m^{-3}, LH power ~250-350kW

When the B_t direction is reversed, striations are *below* and not above the center of each waveguide row

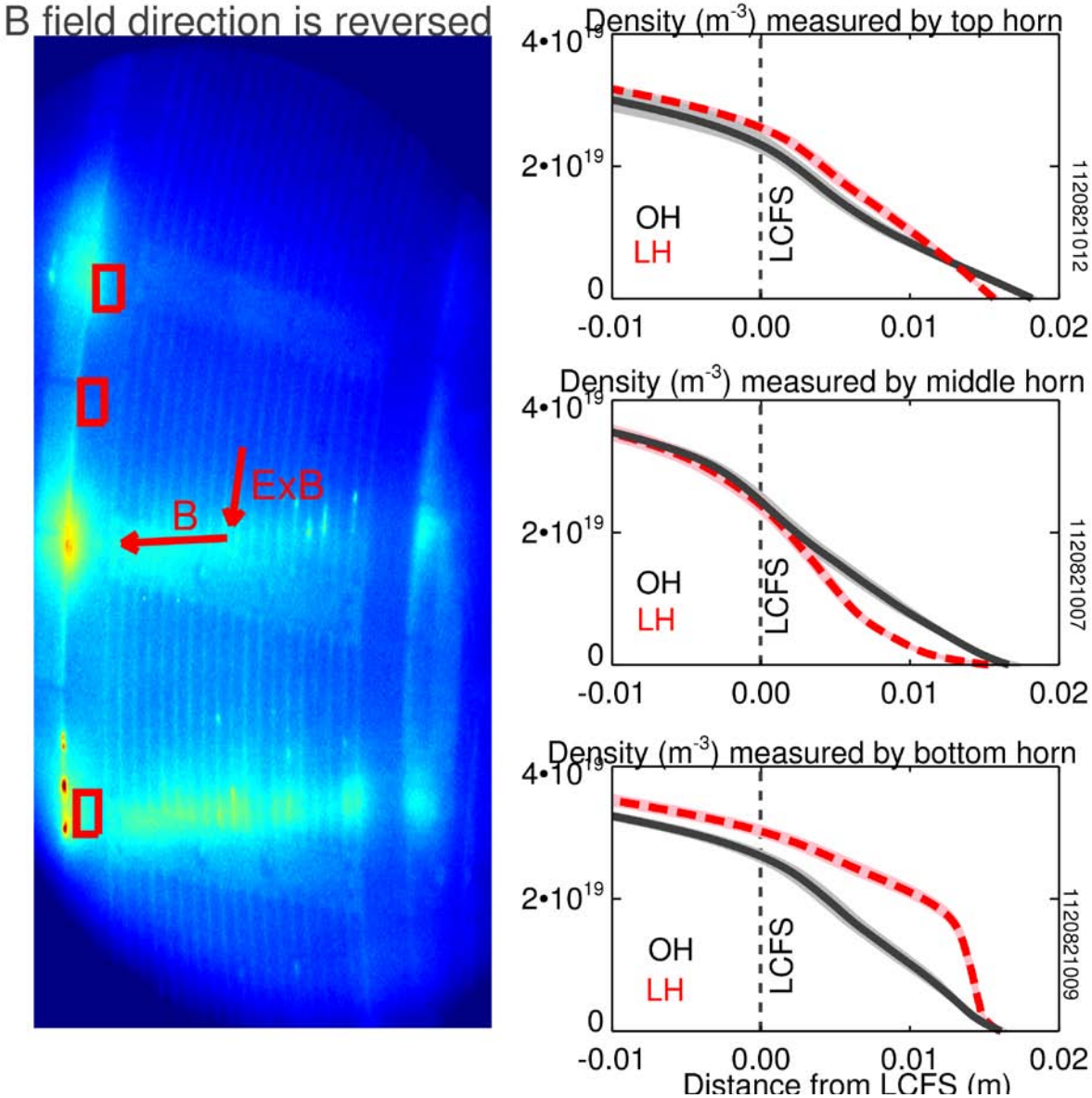

- Reversing toroidal magnetic field causes:
  - Reverseal of ExB convective eddies
  - little to no modification at top horn
  - strong density *decrease* at middle horn
  - strong density *increase* at bottom horn

$\bar{n}_e$ =.55-.7x10^{20} m^{-3}, LH power ~600-800kW

GPI diagnostic is used to measure radial profile of the poloidal phase velocity

- GPI is a 4 cm x 4cm poloidal and radial array that measures emission fluctuations from the resulting plasma turbulence
- GPI is magnetically connected to LH launcher
- Power spectrum can be examined as a function of frequency and poloidal wavenumber, k_θ
- Color scale is normalized for each frequency, so that higher frequency features are resolved
- Slope of line represents positive or negative poloidal phase velocity (upwards or downwards)

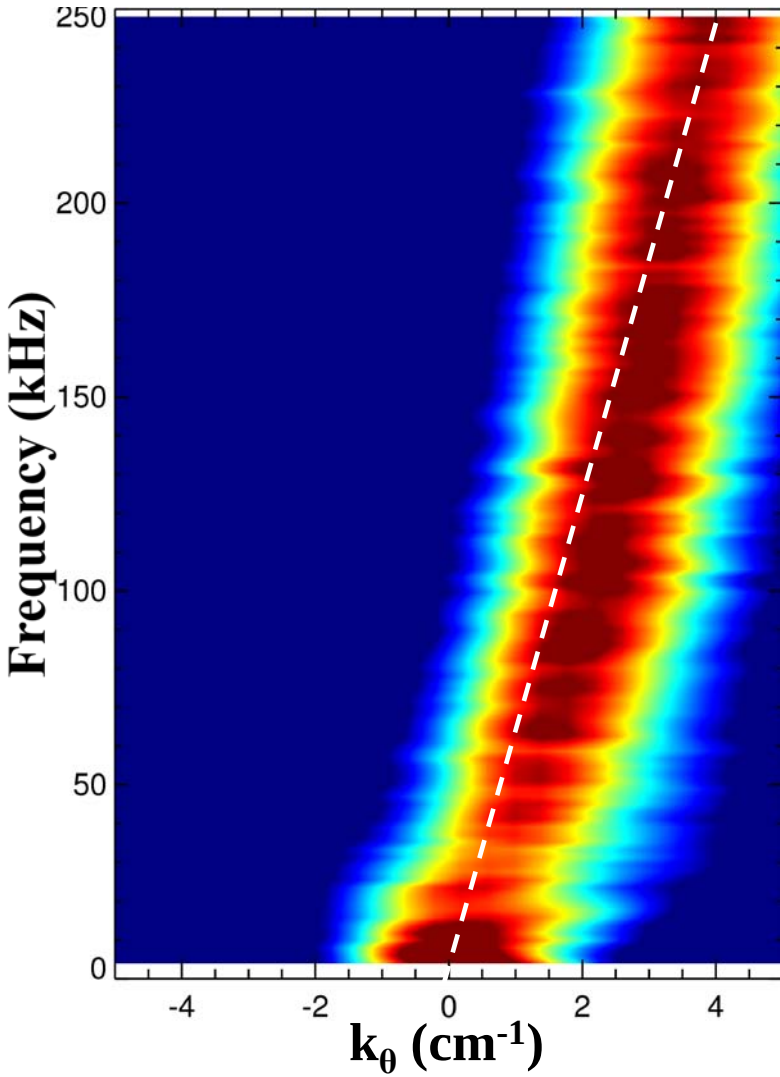

Results indicate LH-induced flow is upwards, changes with $\bar{n}_e$, and consistent with video camera images.

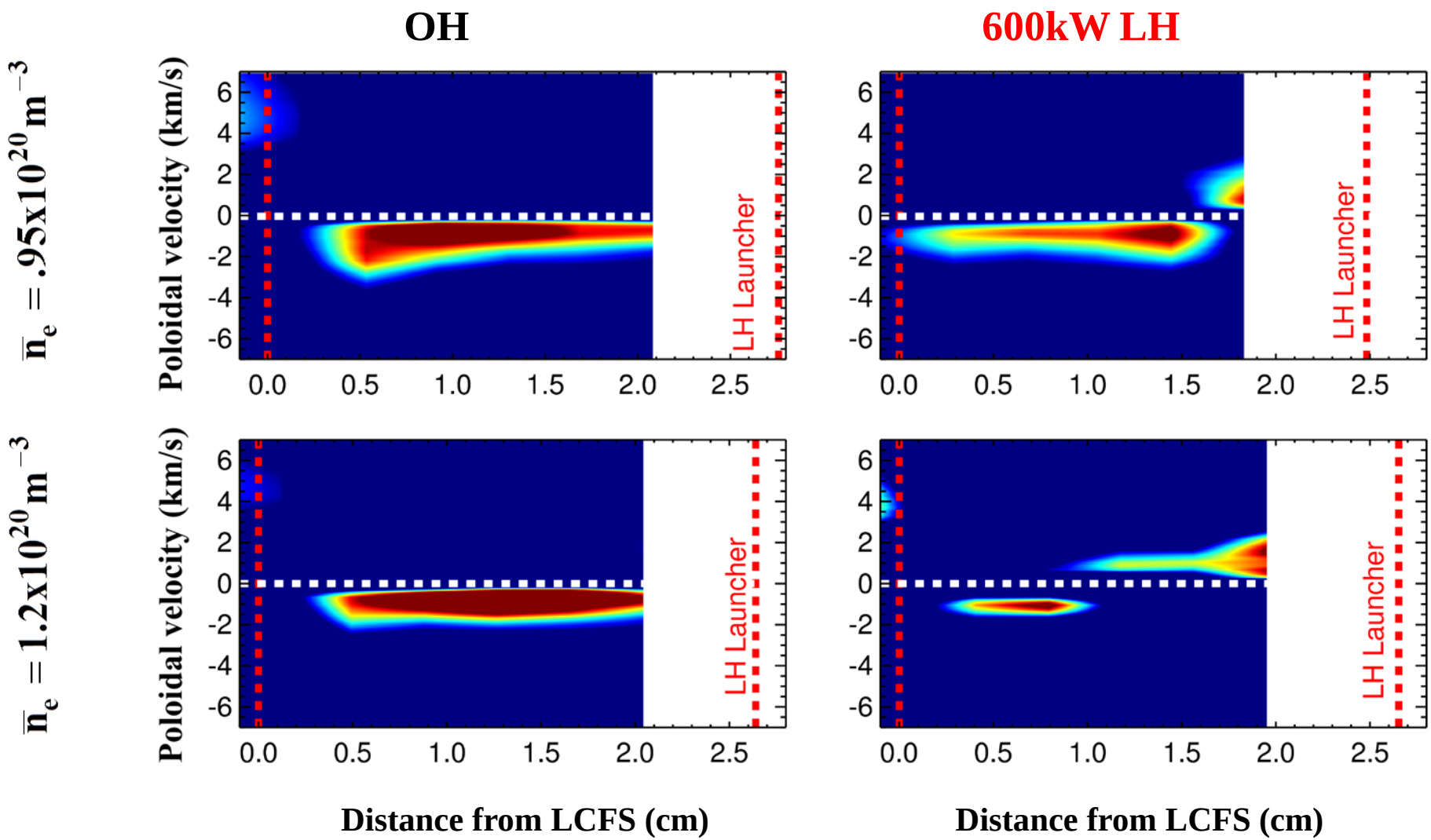

2-D diffusive-convective model is developed to study the impact of LH-induced ExB drifts on SOL density profiles

$$\cancel{\frac{\partial n}{\partial t}} + \nabla \cdot (n\vec{u} - D\nabla n) + \frac{n}{\tau_{\parallel}} = \cancel{\sum n n_j \langle \sigma \vec{u} \rangle_j}$$

$$\vec{u} = \frac{-\nabla V x B}{B^2}$$

$$V = 0 \qquad \text{during OH}$$

$$V = V_{max} e^{-|r-r_0|/L} \sum_{i=1}^{64} \cos\left(\frac{\pi(z - z_i)}{h}\right) \text{ during LH}$$

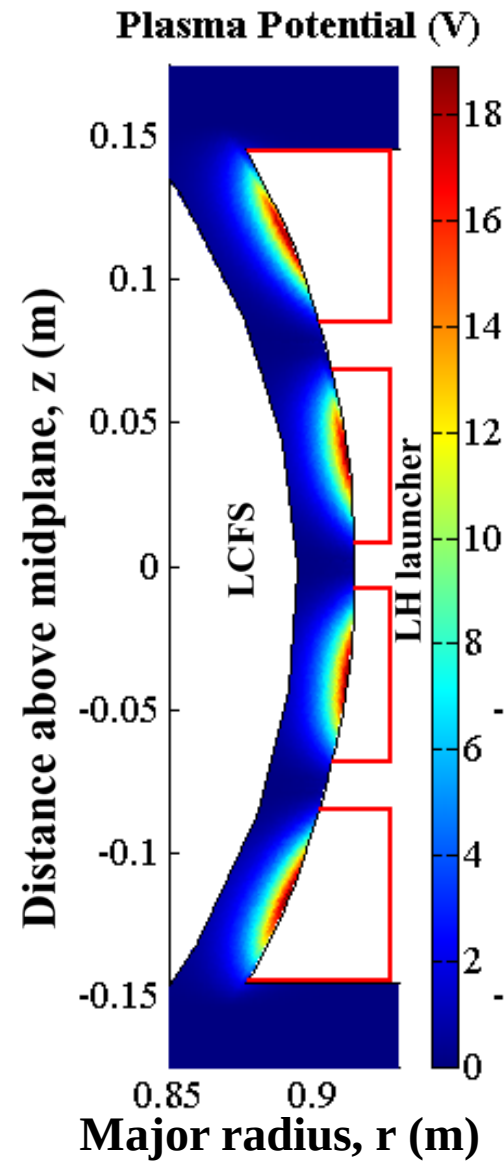

- D and $\tau_{\parallel}$ is assumed to be the same for both OH and LH cases
- Solved using FEM in COMSOL multiphysics package
- z variation of V assumed to be ~E_{LH} (cosine for TE_{10})
- r variation of V is roughly based on GPI measurements and assumption that peak occurs near LH launcher
- Boundary conditions are n=0 at LH launcher, n=constant at LCFS, flux=0 at top/bottom.

The simulated density with convective flow reproduces observed LH-induced striations

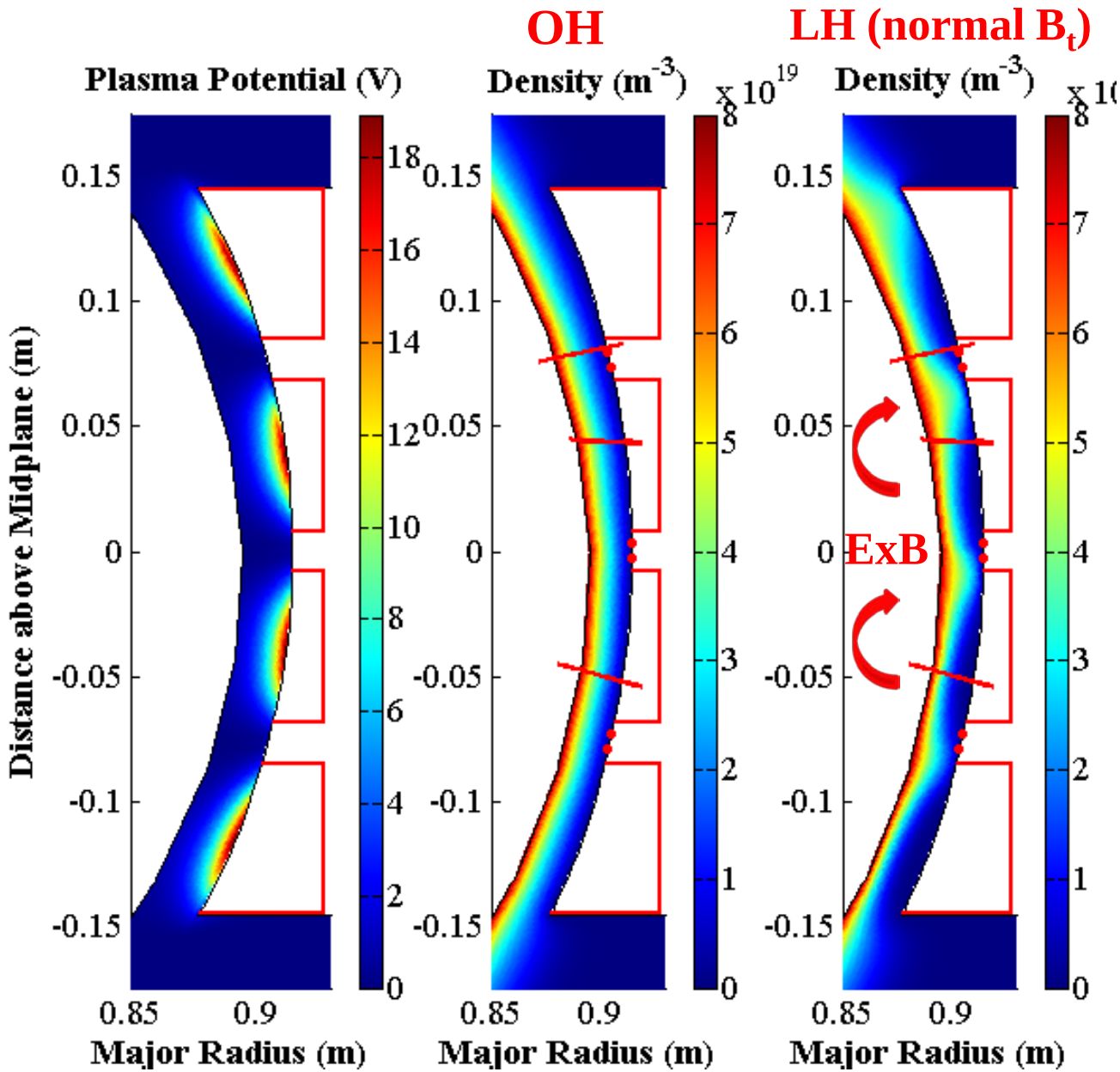

The simulated density with convective flow reproduces observed LH-induced striations

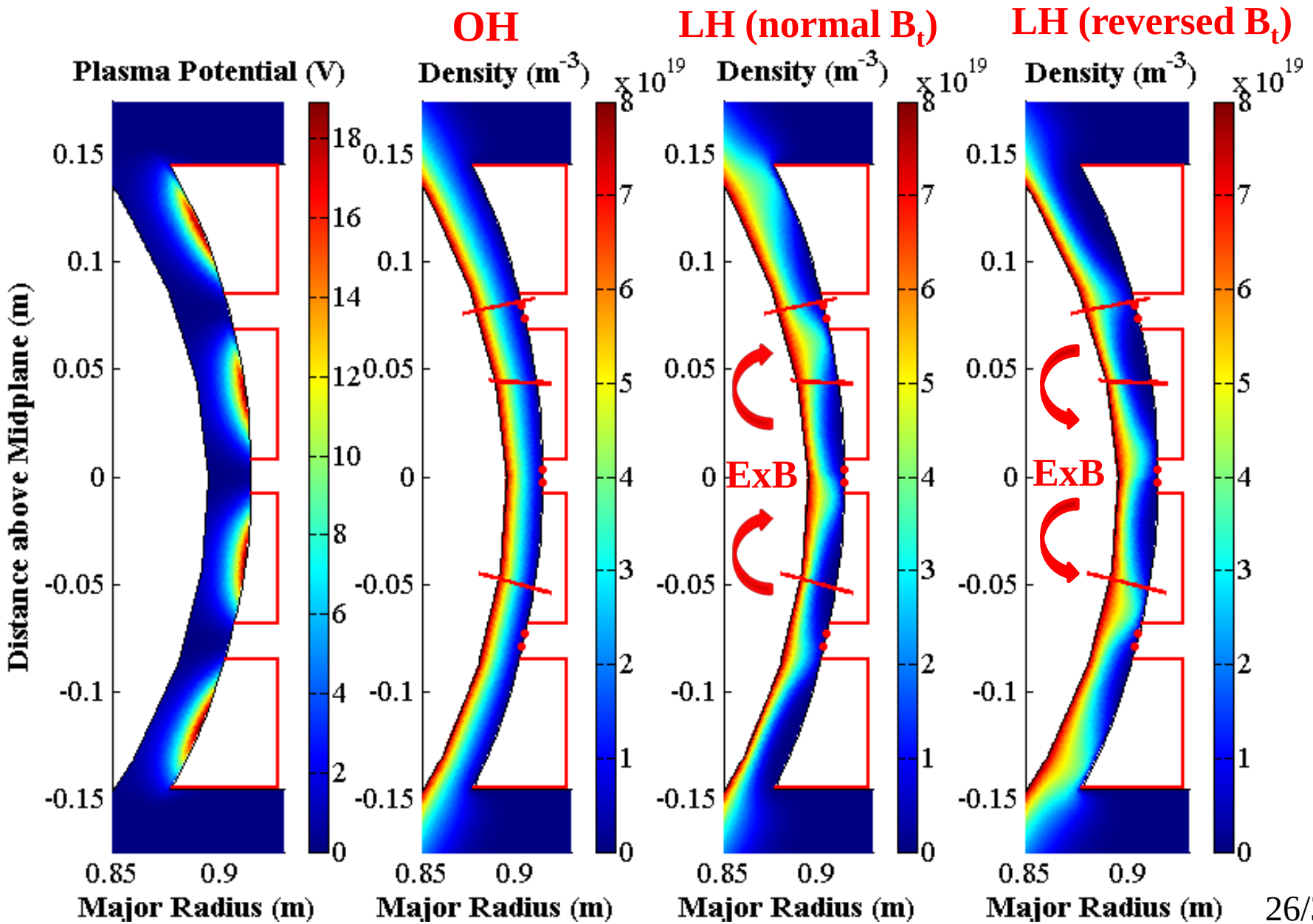

The simulated density reproduces experimental trends along reflectometer sightlines, supporting ExB convective picture

Measured density

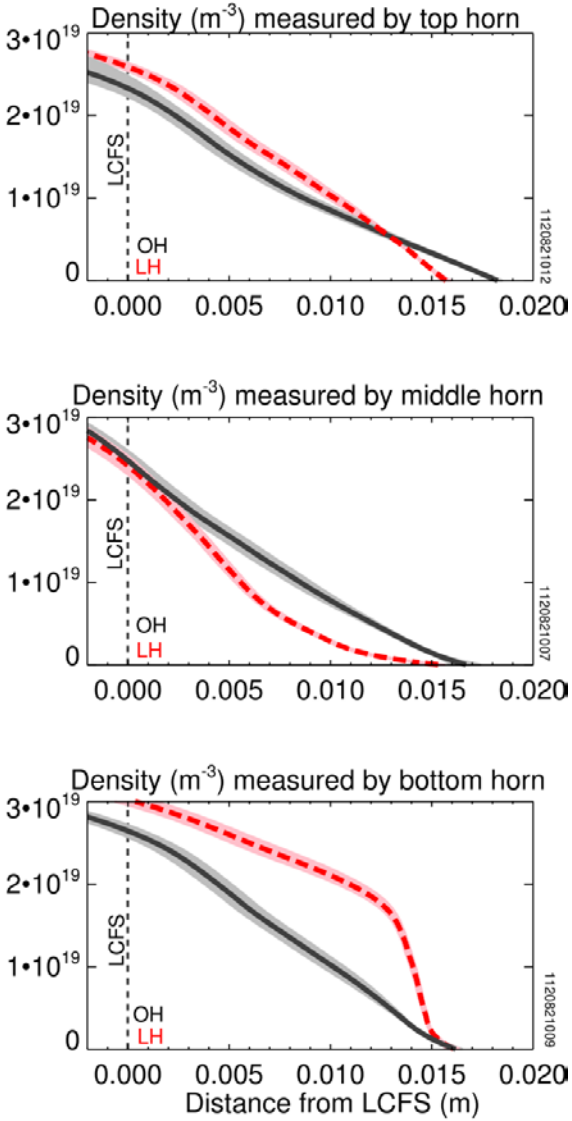

Simulated density

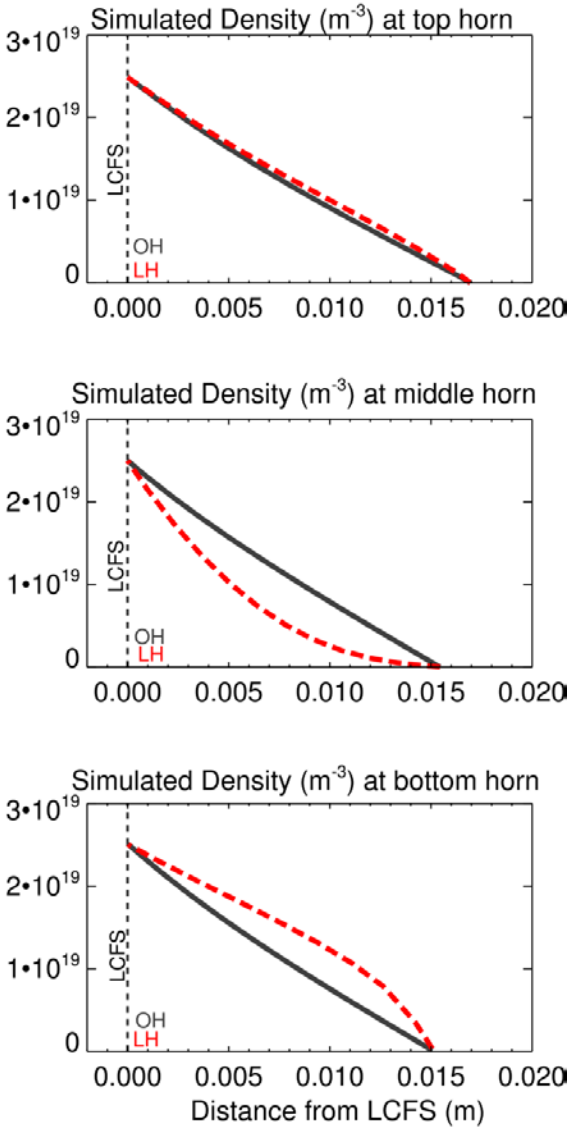

The effect of density profile asymmetries need to be included to understand LH coupling

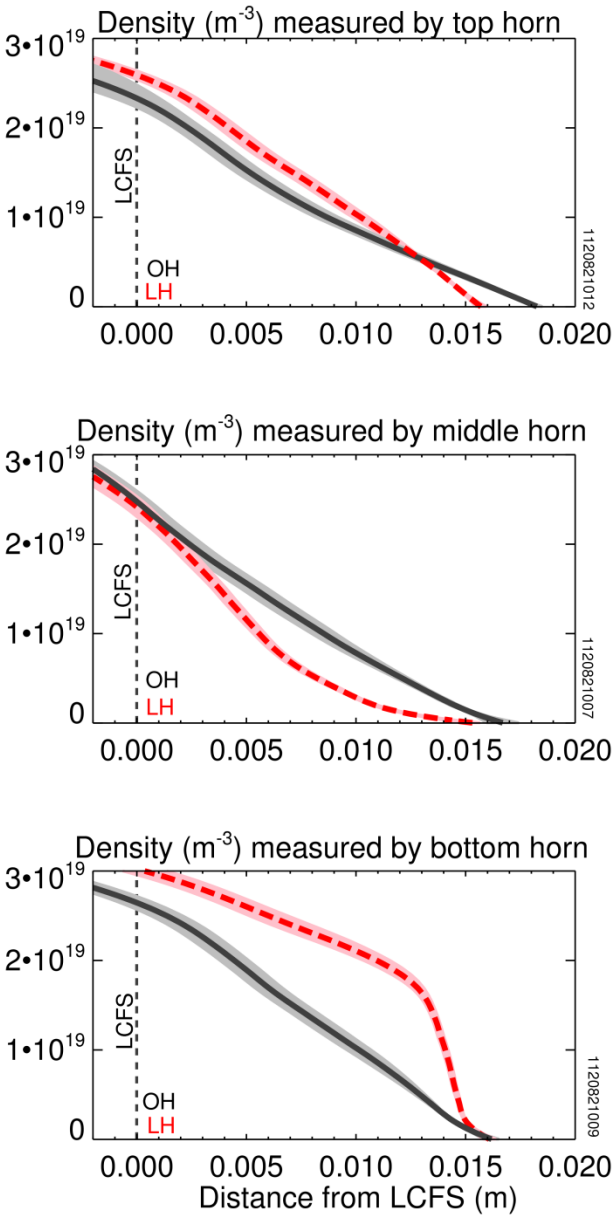

- 2D slab LH coupling model[1] was used to evaluate simulated LH reflection coefficients for top, middle, and bottom horn in the reversed field case

Density Profile used	OH	LH
Top horn	14%	12%
Middle horn	11%	27%
Bottom horn	8%	17%

- Experimental reflection coefficient is 26%
- Poloidal variation of density is important for to get agreement between simulation and experiment
- Simulation also reproduces results of low LH power (few watts) coupling experiments[2]

[1] Shiraiwa, AIP 2009, [2]Meneghini, AIP 2011

Table of Contents

- Why we study RF-SOL interactions and LH coupling?
- X-mode SOL reflectometer density profile measurement
- Effects of LH power on SOL density profiles and LH coupling
- Effects of LH+ICRF power on SOL density profiles and LH coupling

Spatial structure of ICRF-induced plasma potentials

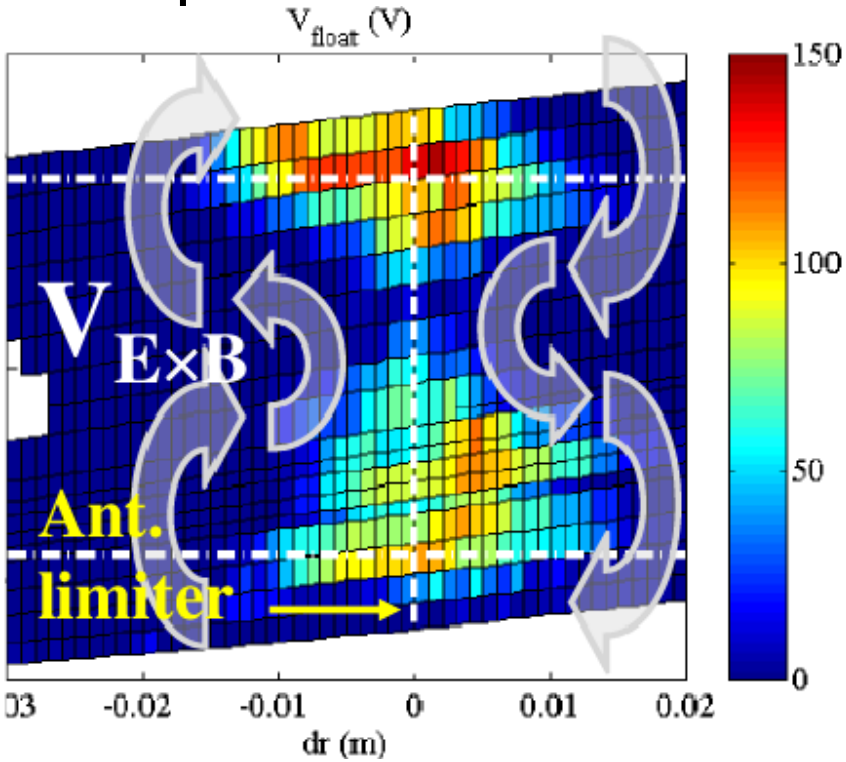

- Complicated spatial structure of ICRF-induced plasma potentials on Tore Supra[1] (shown on left) and Alcator C-Mod[2]

[2]Cziegler et al, PPCF 2012, [3]K K Kirov et al, PPCF 2009, [4]Colas et al, PPCF 2007, [5]Lau et al, submitted to PPCF, [6]Kong et al, PPCF 2012

Spatial structure of ICRF-induced plasma potentials

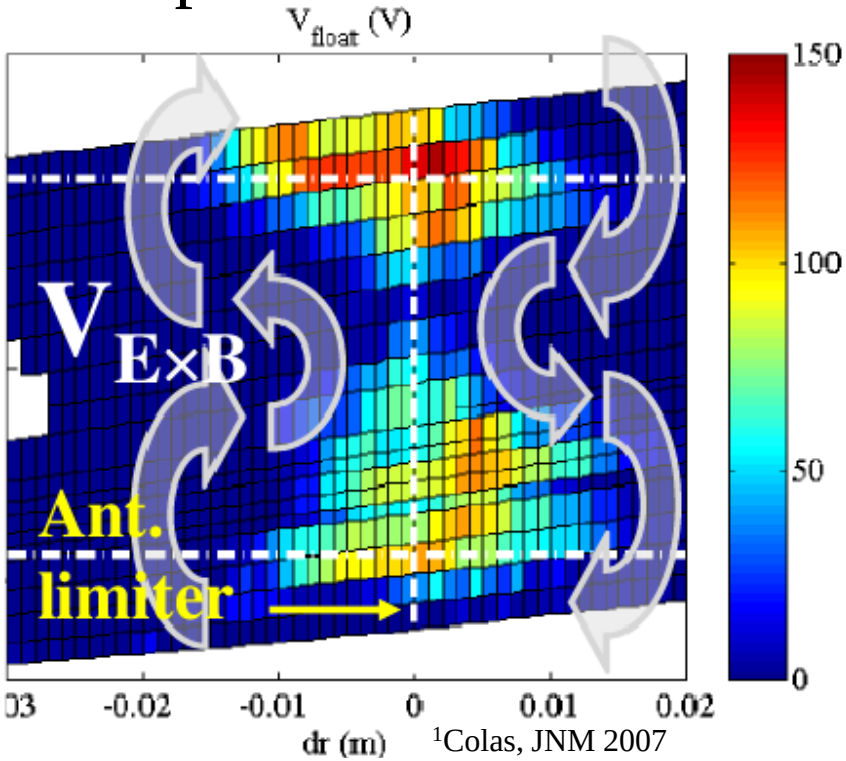

[1]Colas, JNM 2007

- Complicated spatial structure of ICRF-induced plasma potentials on Tore Supra[1] (shown on left) and Alcator C-Mod[2]
  - Magnetic field line mapping and spatial structure of ICRF-induced potential is believed to be important in explaining ICRF-induced LH coupling modifications on JET[3], Tore Supra[4], Alcator C-Mod[5], and EAST[6]
  - first measurement of ICRF-induced poloidal SOL density variations are consistent with LH coupling results

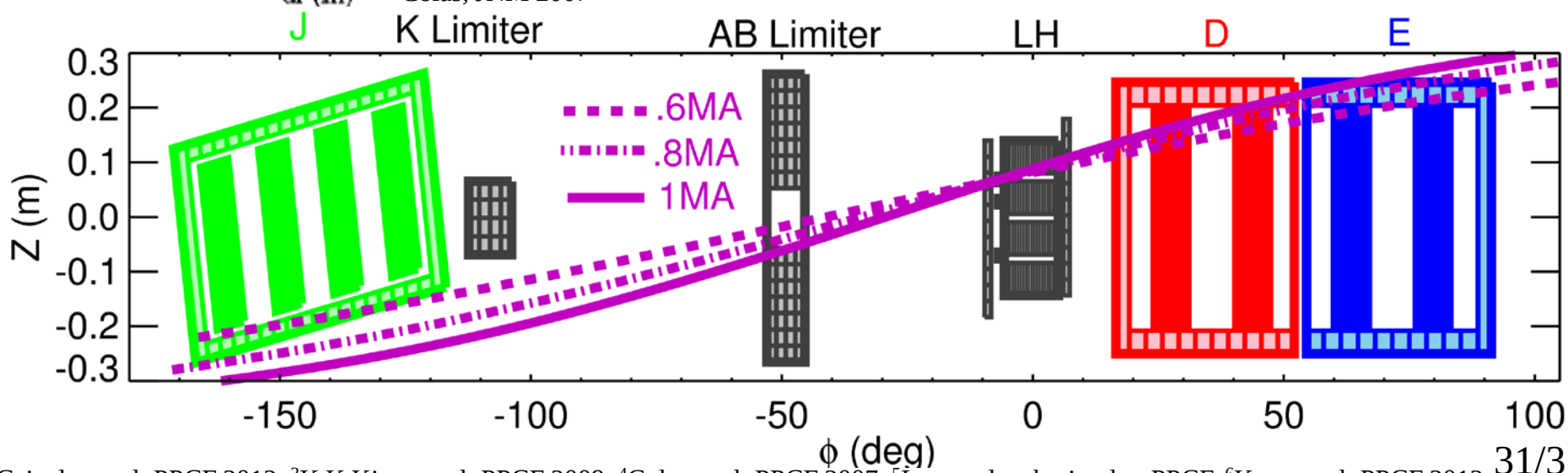

[2]Cziegler et al, PPCF 2012, [3]K K Kirov et al, PPCF 2009, [4]Colas et al, PPCF 2007, [5]Lau et al, submitted to PPCF, [6]Kong et al, PPCF 2012

Dedicated experiment studies effects of ICRF power on LH coupling

- during each discharge, only timing of ICRF and LH power is modified, so that there are time intervals of LH, LH+D, LH+E, and LH+J operation

- $\bar{n}_e$, I_p, outer gap, LH launcher location , and ICRF antenna order was changed between discharges.

- 13 useful discharges were collected with LH reflection coefficients and local measurements of reflectometry density profiles at top horn, and visible video camera images at LH launcher

- trends in LH coupling with LH, LH+D, LH+E, and LH+J held for all discharges

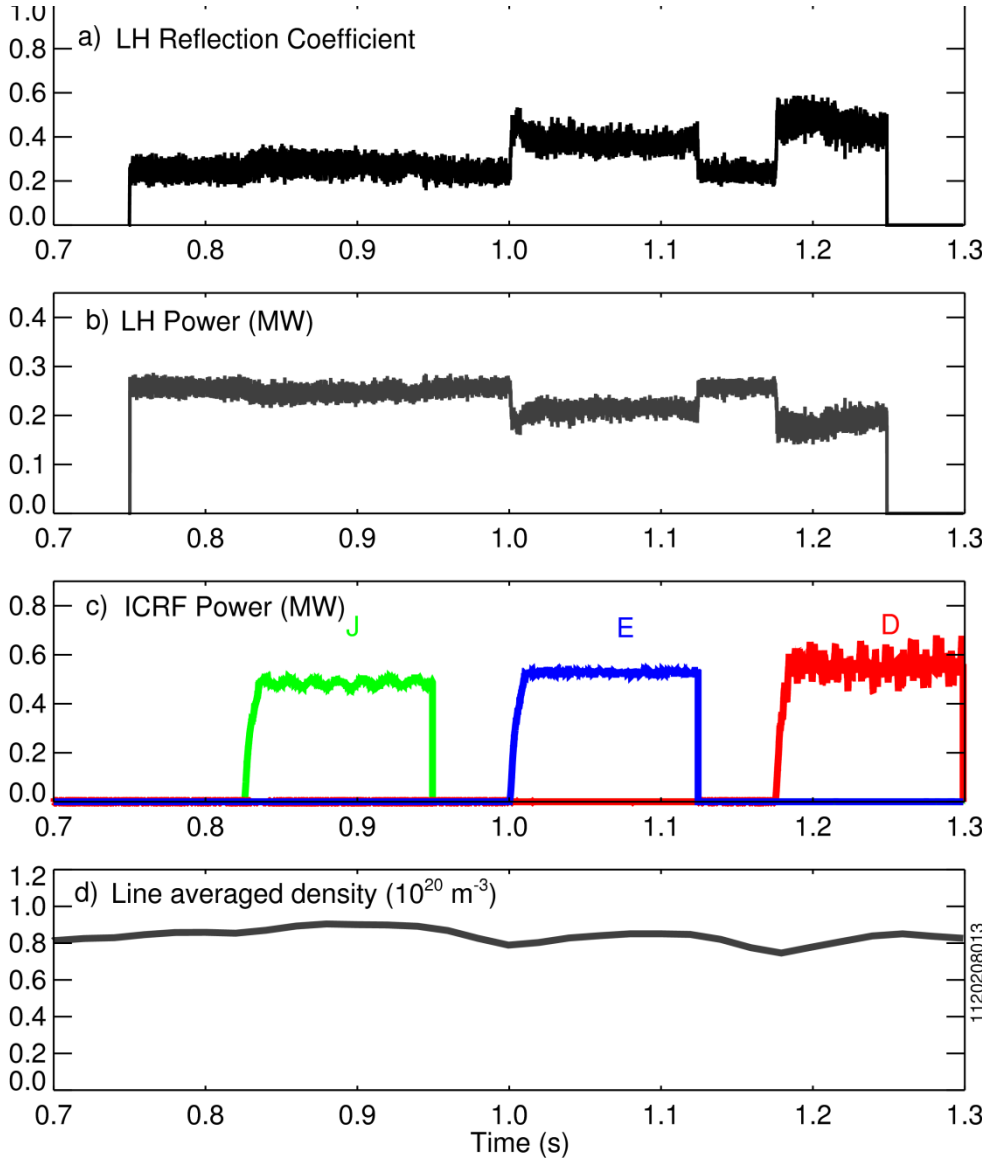

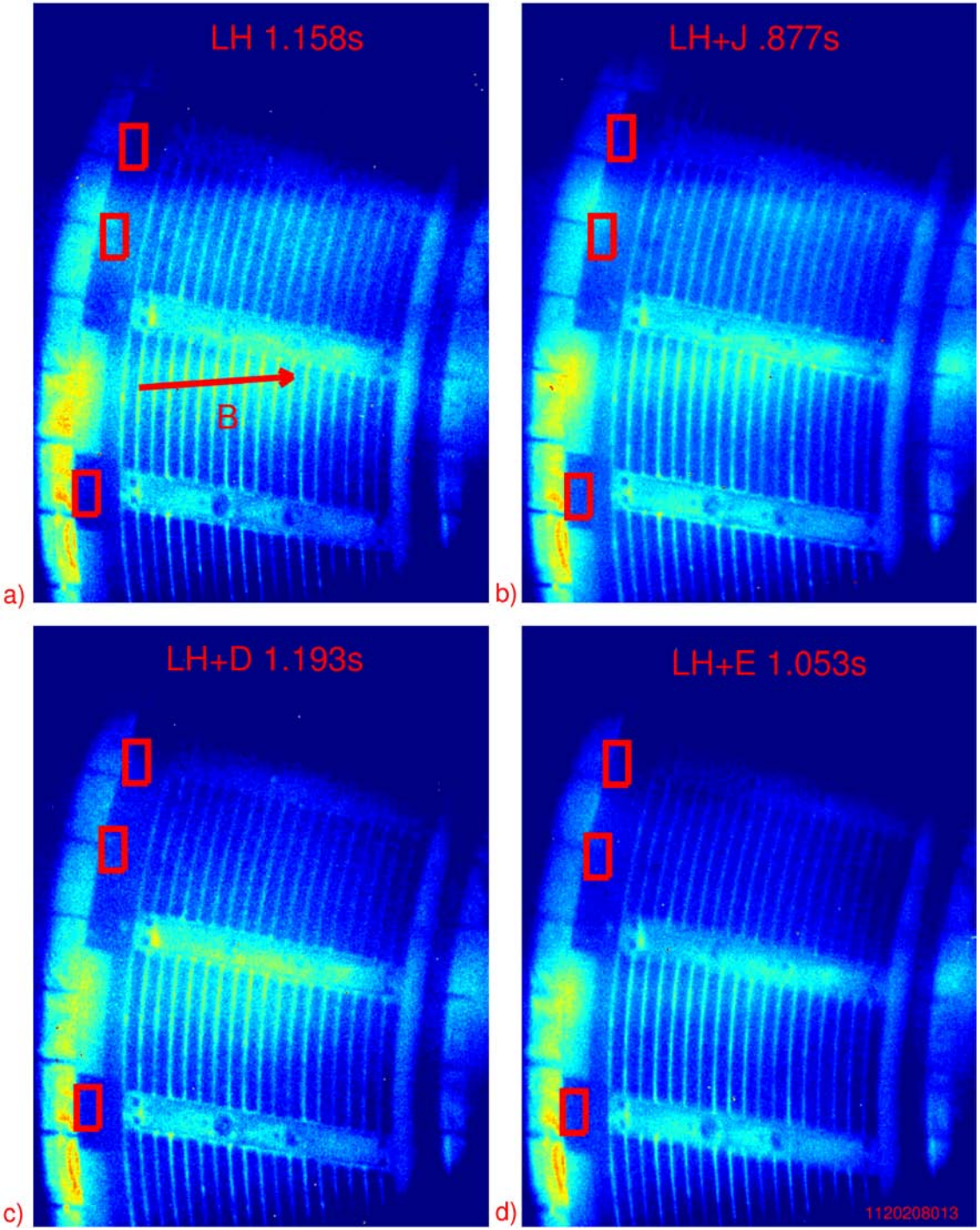

Images show poloidal variation of brightness with LH and LH+ICRF

- Striations above center waveguide in LH operation due to LH-induced flows
- Minimal modification in LH+J operation
- Striation on top-middle waveguide disappears during LH+D and LH+E operation, and may be the cause of reduced LH coupling
- Top and middle horn reflectometer measurements do reflect these observations

Reflectometer measurement at top horn during LH and LH+ICRF operation shows minimal change

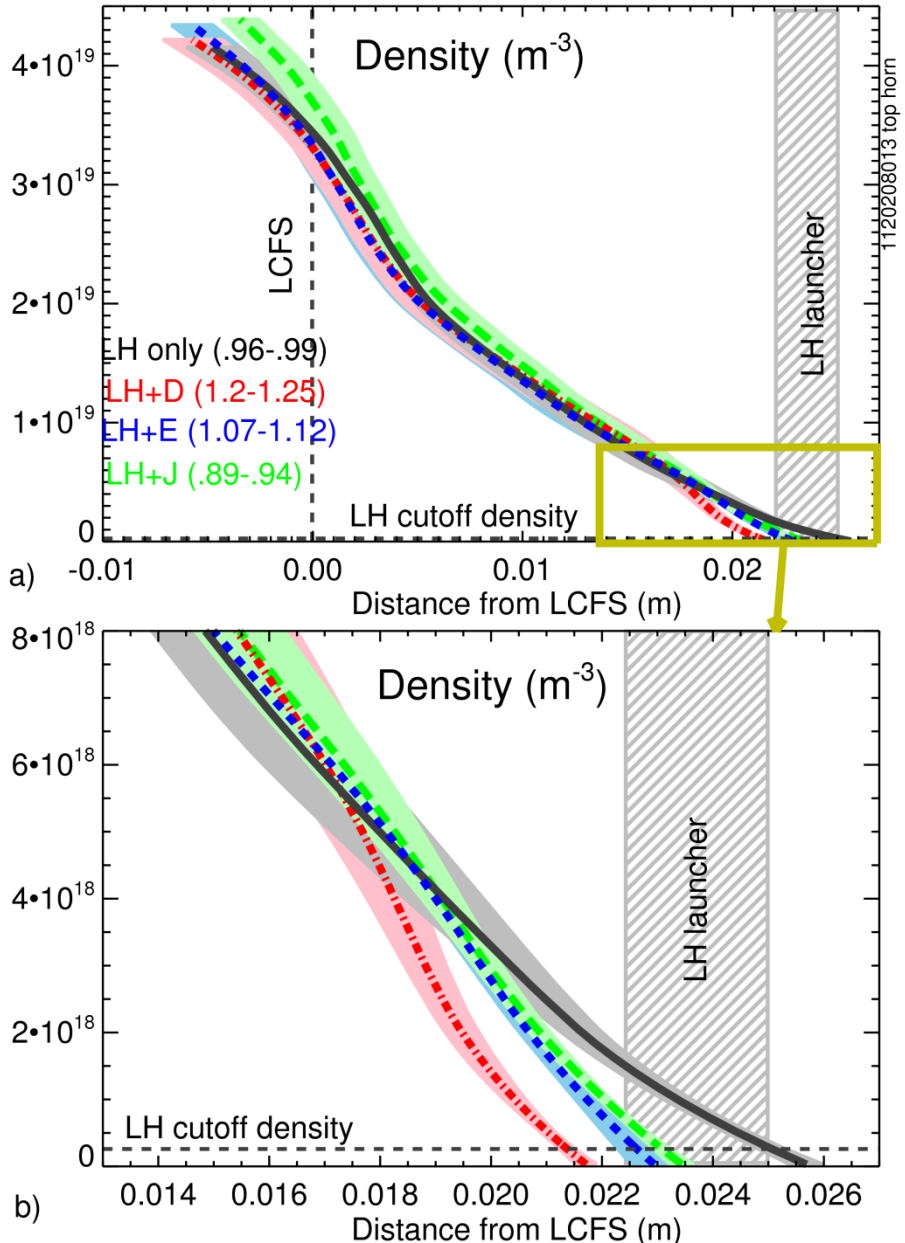

- No significant modification of density at top horn in near SOL
- For a few mm in front of LH launcher, addition of ICRF power depletes density for all ICRF antennas
- Depletion is strongest for D ICRF antenna
- Depletion occurs for J ICRF antenna even if antenna is not magnetically connected to top reflectometer horn

Reflectometer measurement at middle horn during LH and LH+D operation shows large change

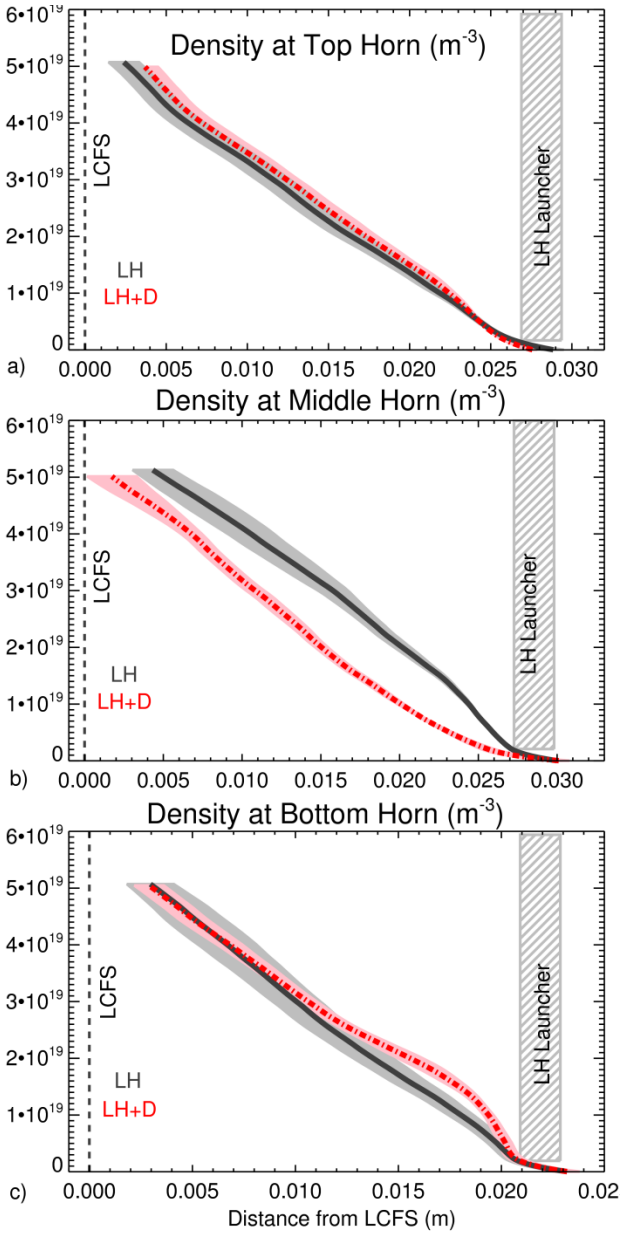

- reflectometer measurements made on separate run day also show minimal difference in density between LH and LH+D at top horn
- significant depletion in density at middle horn during LH+D operation, consistent with video camera images, and LH coupling results
- necessary to understand both LH and ICRF-induced drifts to understand effect on LH coupling during combined LH and ICRF operation

Proposed solutions to improve LH coupling

- past and present setup of localized gas puffing on Alcator C-Mod cannot improve LH coupling without affecting global plasma performance

- will poloidal array of localized gas puff nozzles adjacent to LH launcher improve LH coupling?
  - local density modifications?
  - tailor gas puff to address poloidal density asymmetries?

Video camera during localized gas puffing in OH discharges

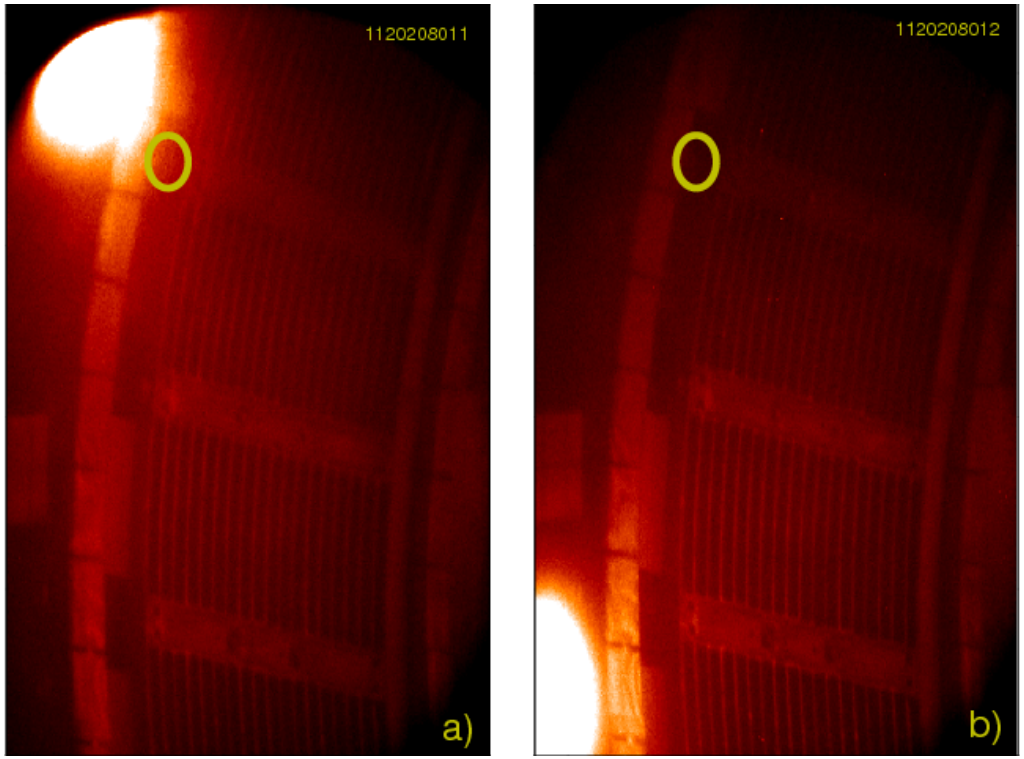

- other possibly useful solutions are:
  - non-adjacent ICRF antennas and LH launchers
  - reducing ICRF sheaths and LH-SOL absorption will require better understanding of these processes

[1] Ridolfini, PPCF 2003

Summary of ICRF and LH effects on SOL density profiles and LH coupling

• design, implementation, and installation of X-mode reflectometer has been used for measurement of density profile in front of LH launcher in a tokamak

- first observation of LH and ICRF-induced SOL density profile modifications and poloidal asymmetries in a tokamak

• diffusive convective model has been developed to study impact of ExB convective eddies on SOL density profiles

- Simulated results reproduces experimental density profiles

• LH coupling model has been used to show the importance of including poloidal density asymmetries in understanding LH coupling

- density in front of waveguide mouth is necessary for simulated LH reflection coefficients to match experimental results

• dedicated measurement detailing the effects of ICRF power on LH coupling confirm that LH coupling degrades with simultaneous operation of LH launcher and adjacent ICRF antenna

- coupling results are consistent with density modifications observed during LH and LH+ICRF operation

Extra Slides

Measured LH-induced density profile modifications are consistent with ExB convective eddies

Numerous possible physical mechanisms for LH-induced density profile modifications proposed:

- SOL ionization[1,2]
- ponderomotive force[3,4]
- ExB convective eddies[5,6]

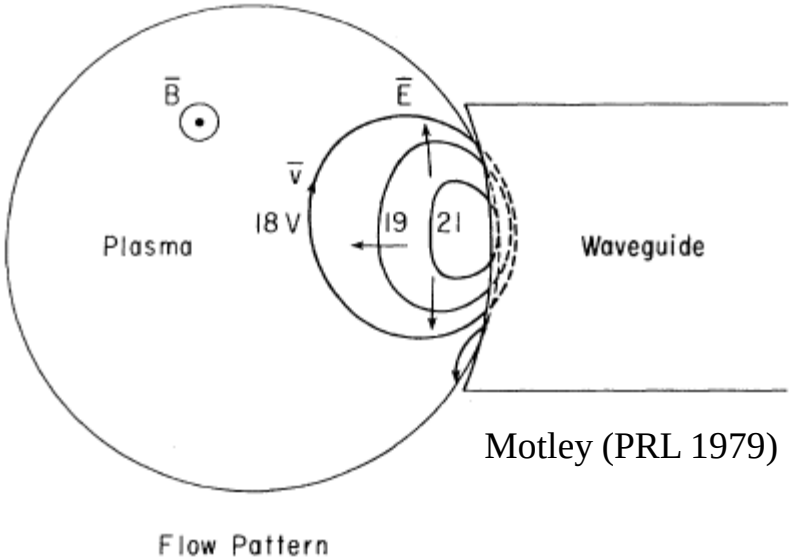

Motley (PRL 1979)

- First local density profile measurements at LH launcher in tokamaks
  - first measurement of LH-induced density radial and poloidal variations
  - LH-induced modifications depend on LH power, B_t direction, inner gap
- Developed diffusive-convective model shows that LH-induced density modifications are consistent with ExB convective eddies.
- LH coupling is shown to be sensitive to poloidal density profile asymmetries

[1]Ekedahl NF2005 [2]Petrzilka NF2011 [3]Petrzilka NF1991 [4]Meneghini AIP2011 [5]Motley PRL 1979 [6]Lau, PPCF 2013

Are these density profile measurements consistent with ICRF sheath physics?

- ICRF can increase or decrease density at different poloidal and radial regions
- ICRF-induced density modifications occur on field lines not mapped to active ICRF antenna, but appear stronger on field lines mapped to active ICRF antenna
- magnitude of simulated density modifications can be substantially larger than experimental density modifications
- simulated ICRF-induced density modifications are sensitive to spatial structure of ICRF-induced plasma potential

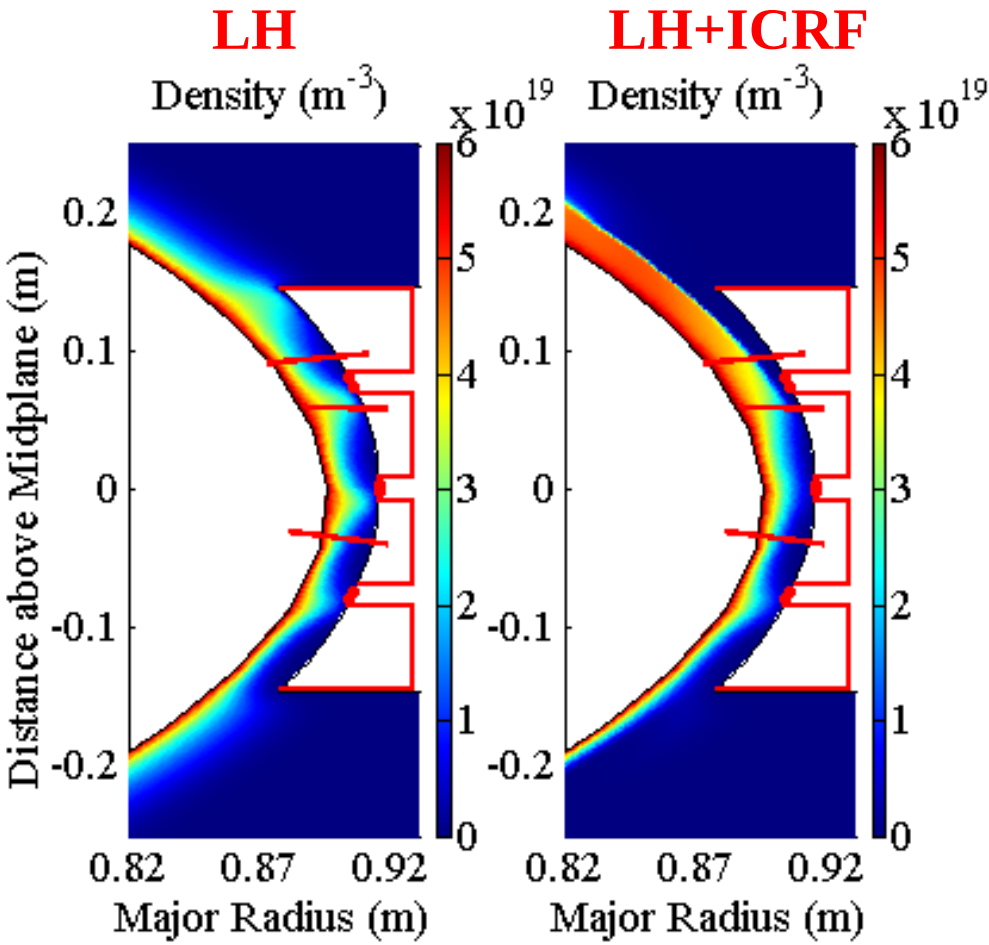

DC sheath potentials in OH plasmas

- On open magnetic field lines in SOL, thermal DC sheath potentials form

$$V \sim 3T_e$$

DC sheath potentials in RF plasmas

- On open magnetic field lines in SOL, thermal DC sheath potentials form

$$V \sim 3T_e + V_{ICRF}$$

What happens if we apply a oscillating potential to one end of the field line[1,2]?

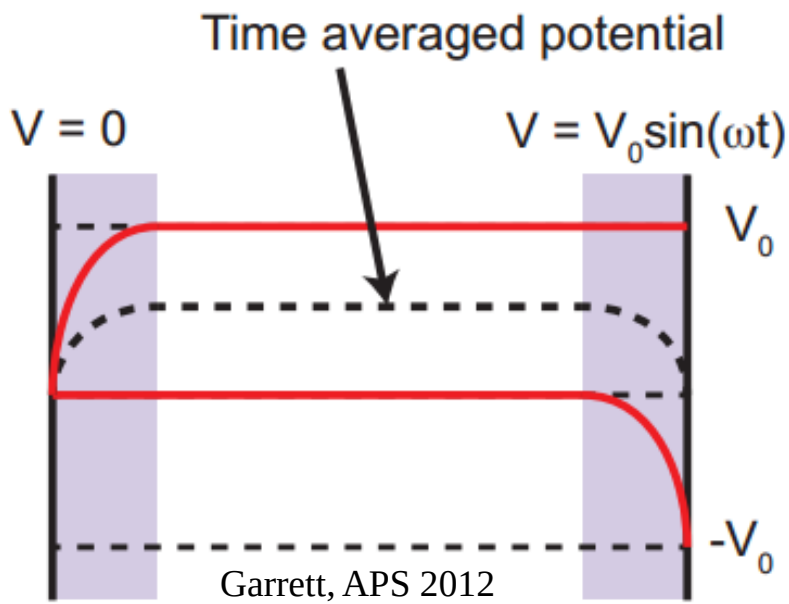

Garrett, APS 2012

- $V_{ICRF} \sim 100\text{-}300V >> 3T_e$
- for ICRF (80MHz):
  - ions respond to time averaged RF electric field[3]
  - electron responds to instantaneous RF electric fields.
- for LH (4.6GHz):
  - ions and electrons both respond to time-averaged fields

[1] D'Ippolito, PPCF 1991 [2] Myra, NF 2005 [3] Lieberman, IEEE 1988

DC sheath potentials in RF plasmas

- On open magnetic field lines in SOL, thermal DC sheath potentials form

$$V \sim 3T_e$$

For LH range of frequencies, other processes can contribute:

What happens if RF power heats up the thermal electrons?

- higher T_e => higher V

What happens if RF power creates a non-thermal electron population?

- equations need to be resolved with non-Maxwellian electron population
- presence of a small population of fast electrons (.1%) can double V[1]

RF-induced SOL absorption[2] can lead to higher sheath potentials

[1]Tskhakaya, PoP 2002 [2]Wallace, NF 2010

Locations of all diagnostics and systems for this thesis

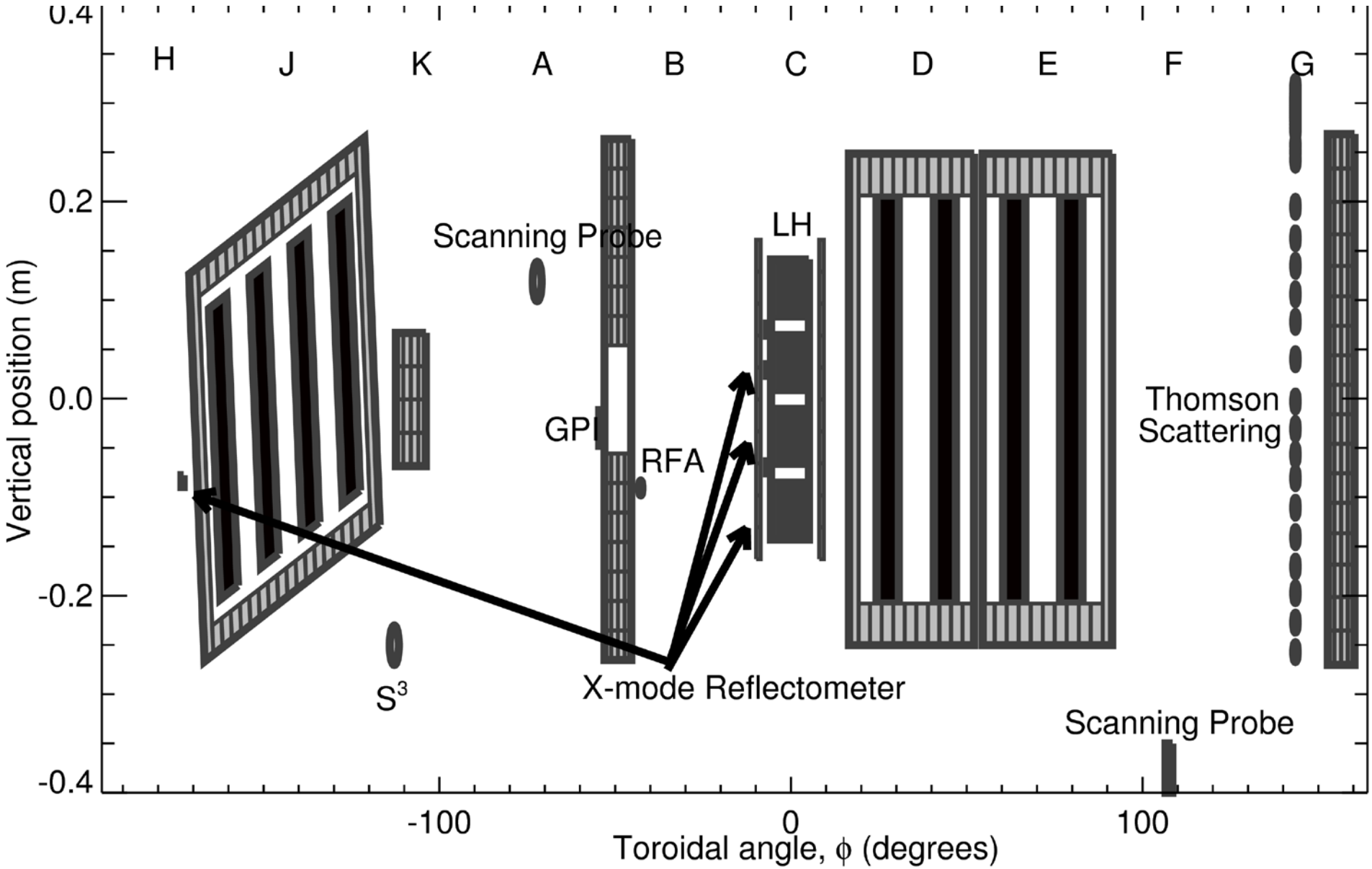

ICRF antennas

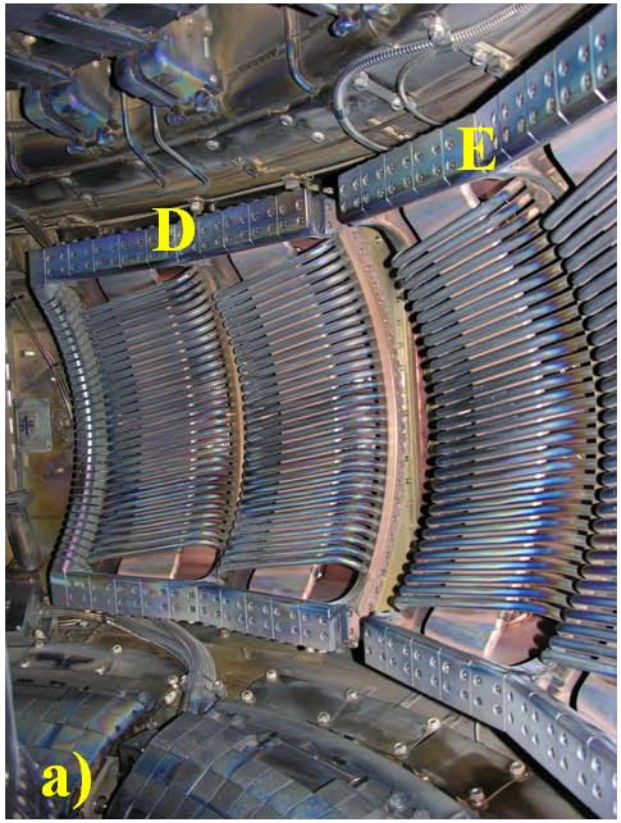

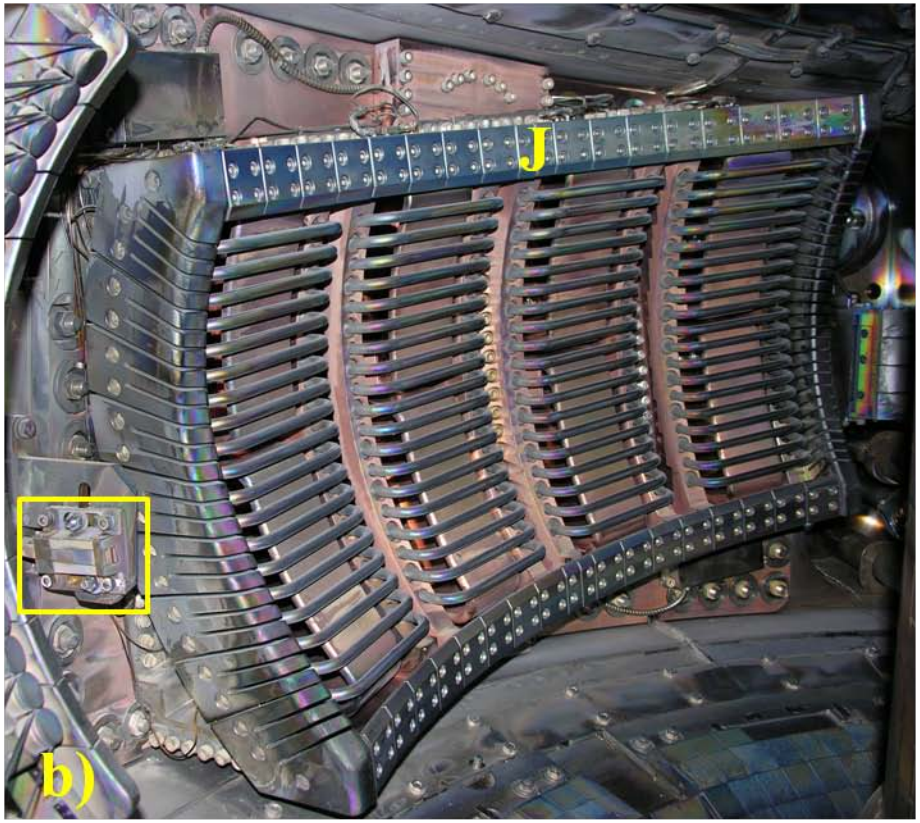

Sputtering yield as a function of sheath voltage (V)

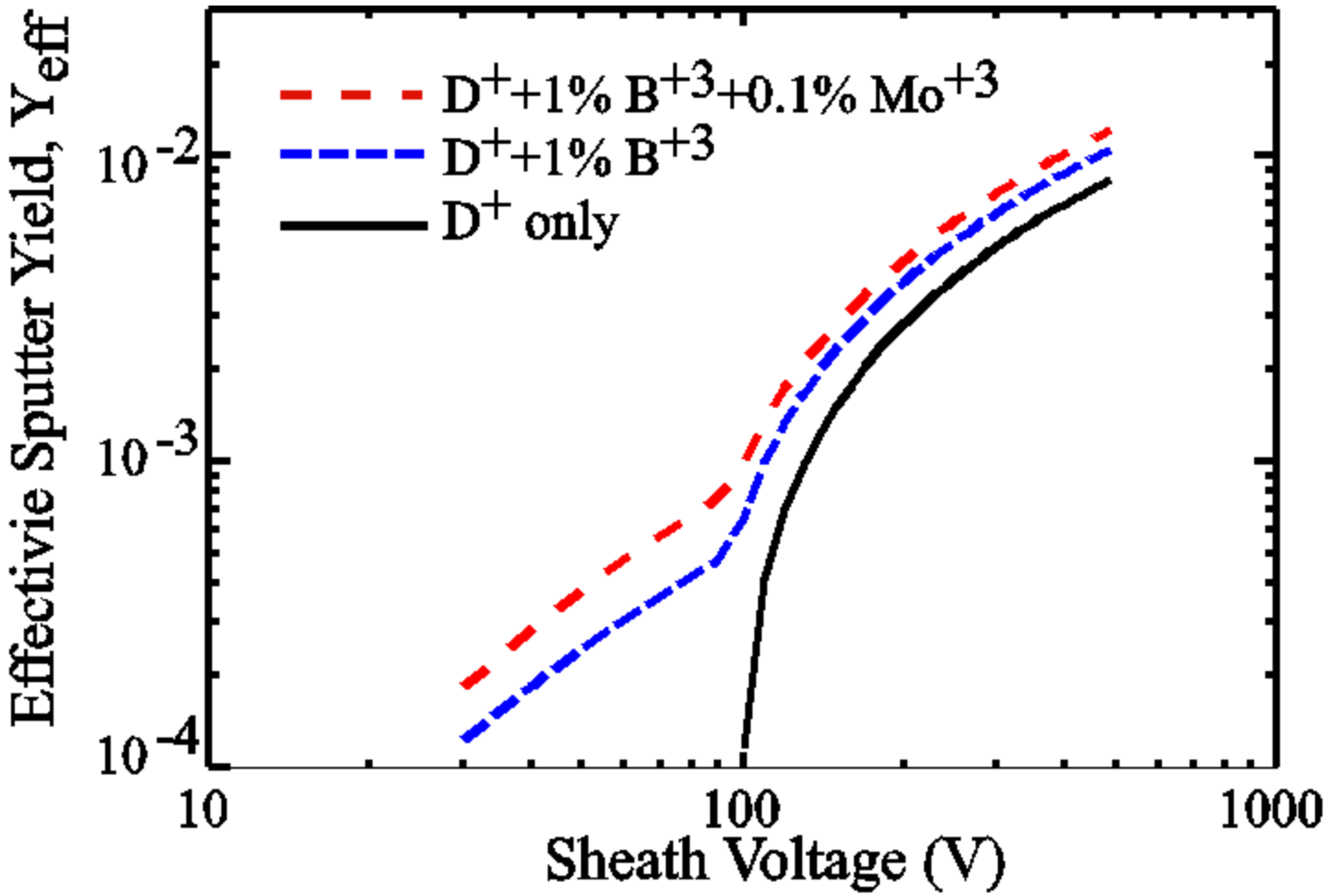

Requires a sheath potential > ~100V for any significant physical sputtering

Reflectometer electronics layout

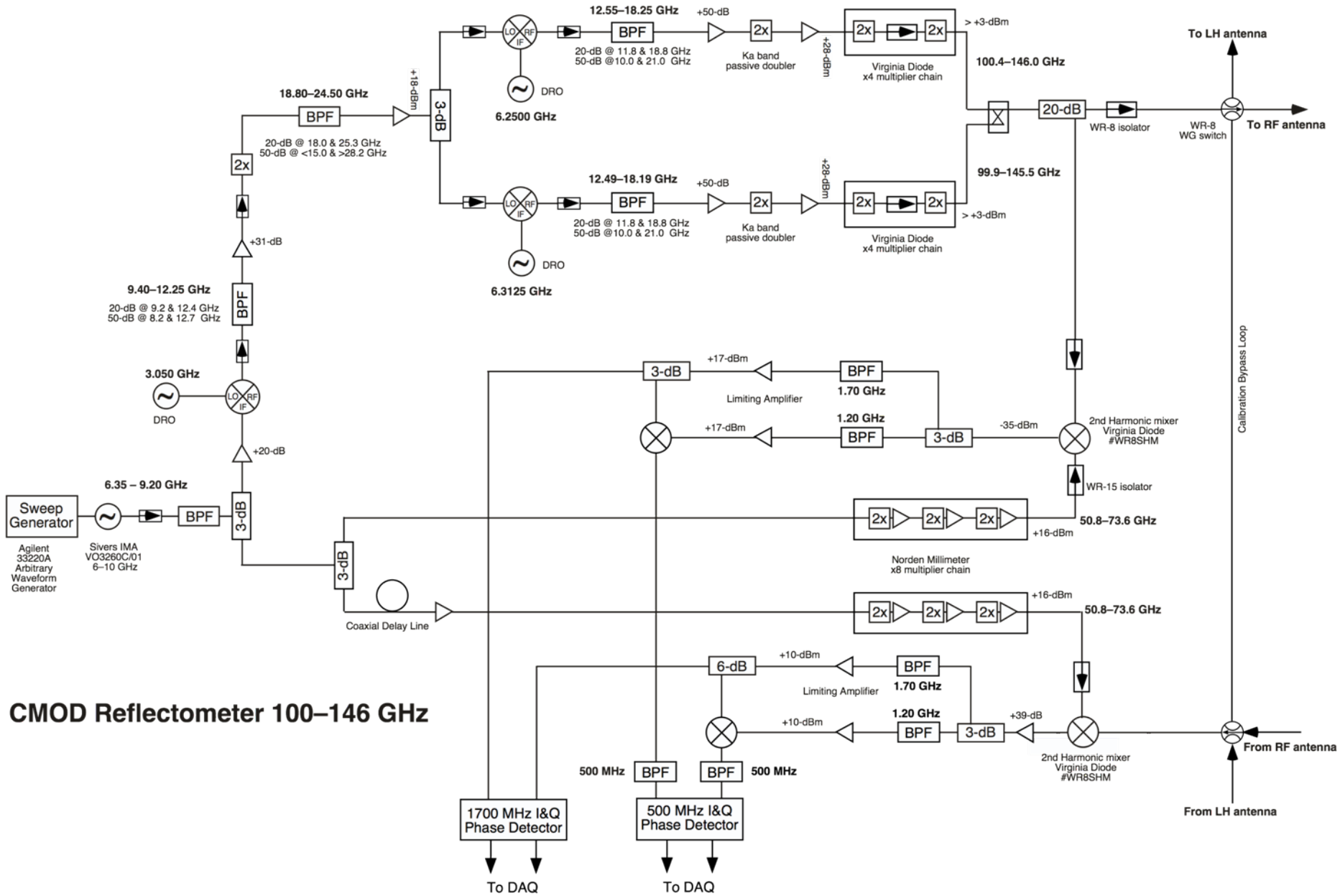

LH “density limit”

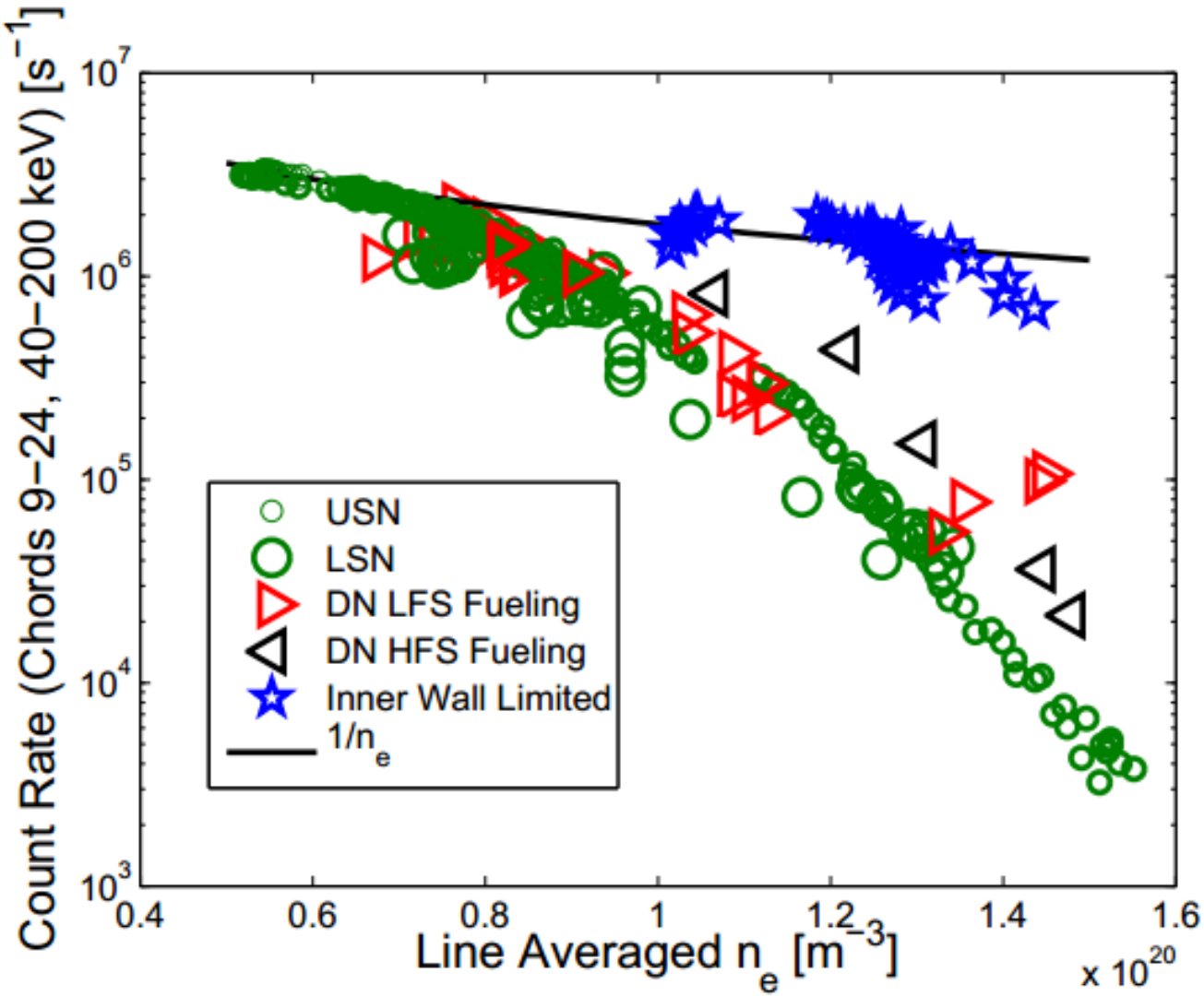

Leading explanations all involve some sort of edge/SOL absorption mechanism

Effect of LH power on SOL density profiles is weaker for smaller inner gaps

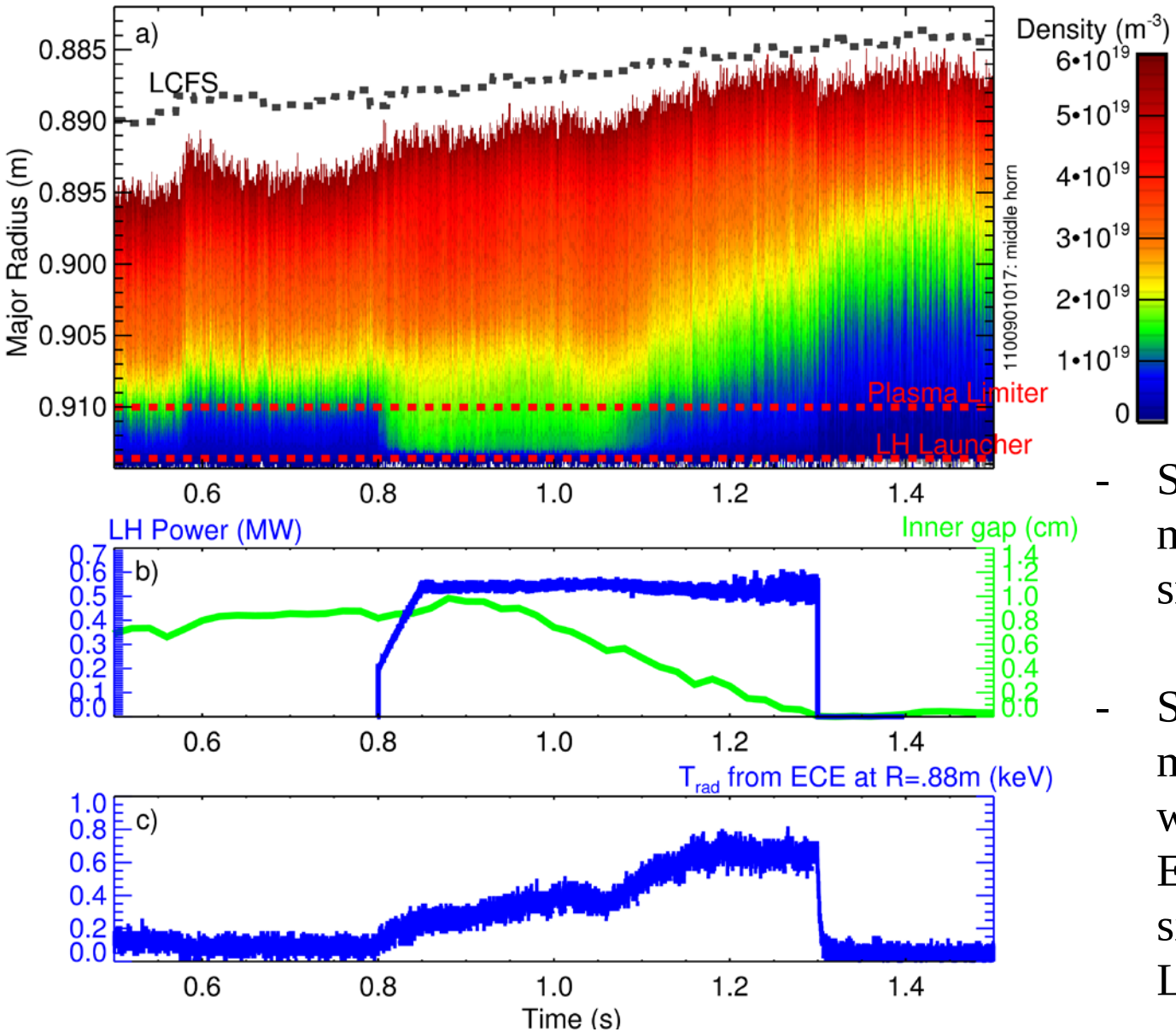

- Smaller density modifications for smaller inner gaps
- Smaller density modifications correlate with increased edge ECE T_{rad} (non-thermal signature and better LHCD efficiency)

For high $\bar{n}_e > 1x10^{20}$ m^{-3} LH discharges, SOL density increases at middle horn *behind* LH launcher

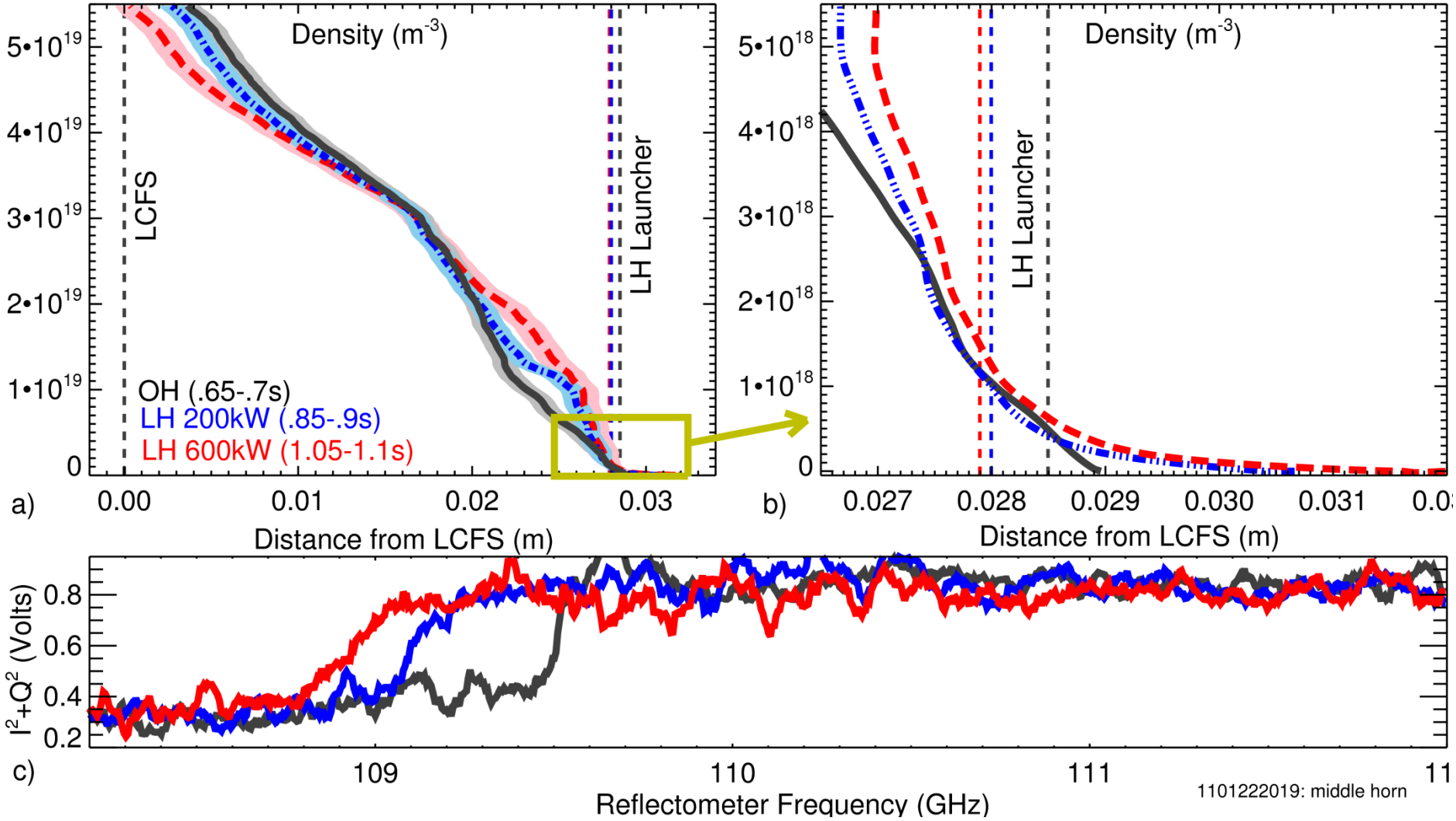

Density increase behind LH launcher only occurs for high $\bar{n}_e$ LH discharges at horn locations near striations

LH-induced striations appear at different toroidal locations on Alcator C-Mod and on different LH experiments

Video camera image of the GH limiter on Alcator C-Mod

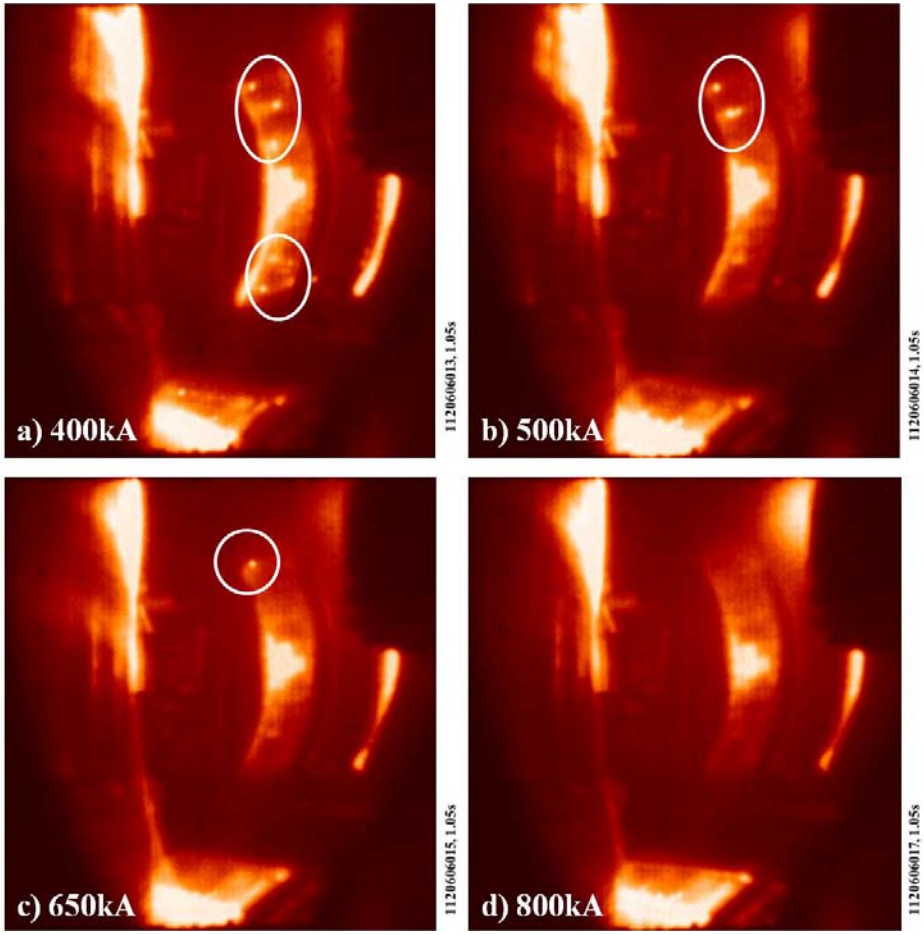

Tronchin-James (2012 Alcator science meeting)

IR Video camera image of the LH launcher on Tore Supra

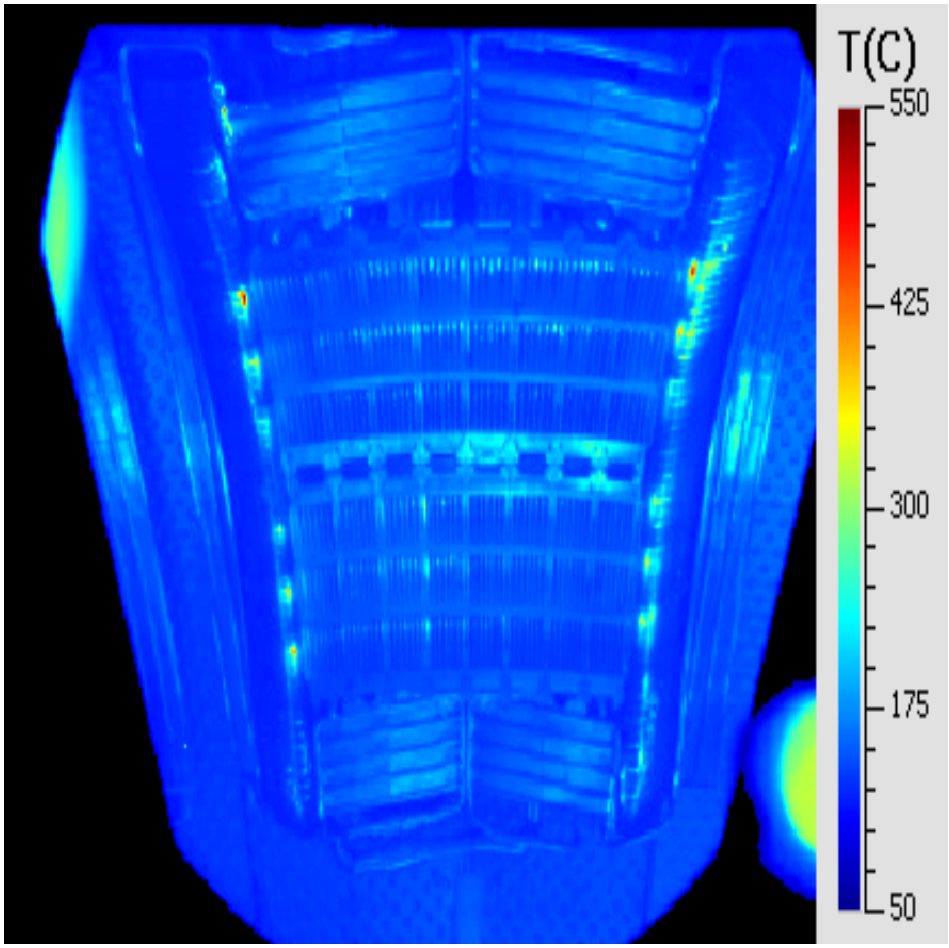

LH Tore Supra group (2012)

Localized gas puffing at top gas nozzle shows small, but noticeable density increase at top horn

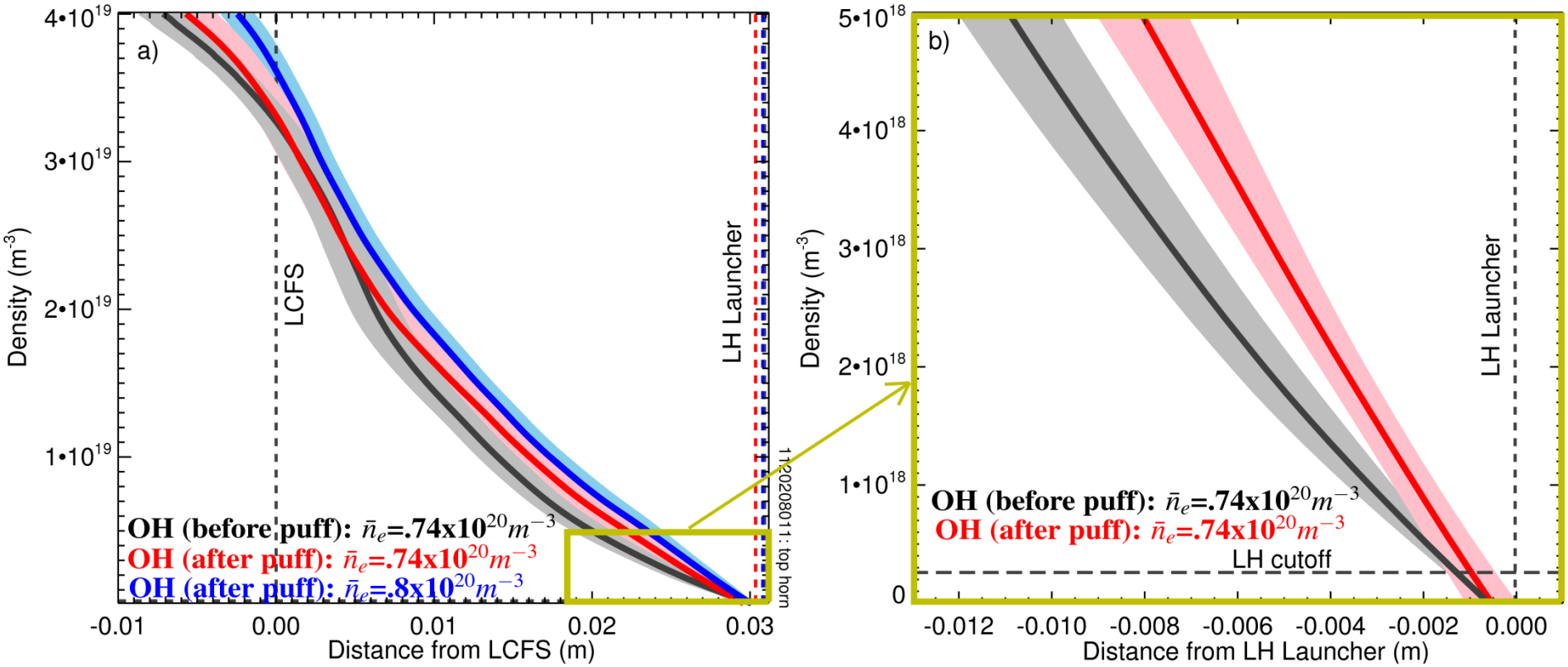

Localized gas puffing at bottom gas nozzle shows negligible difference in density profile at top horn

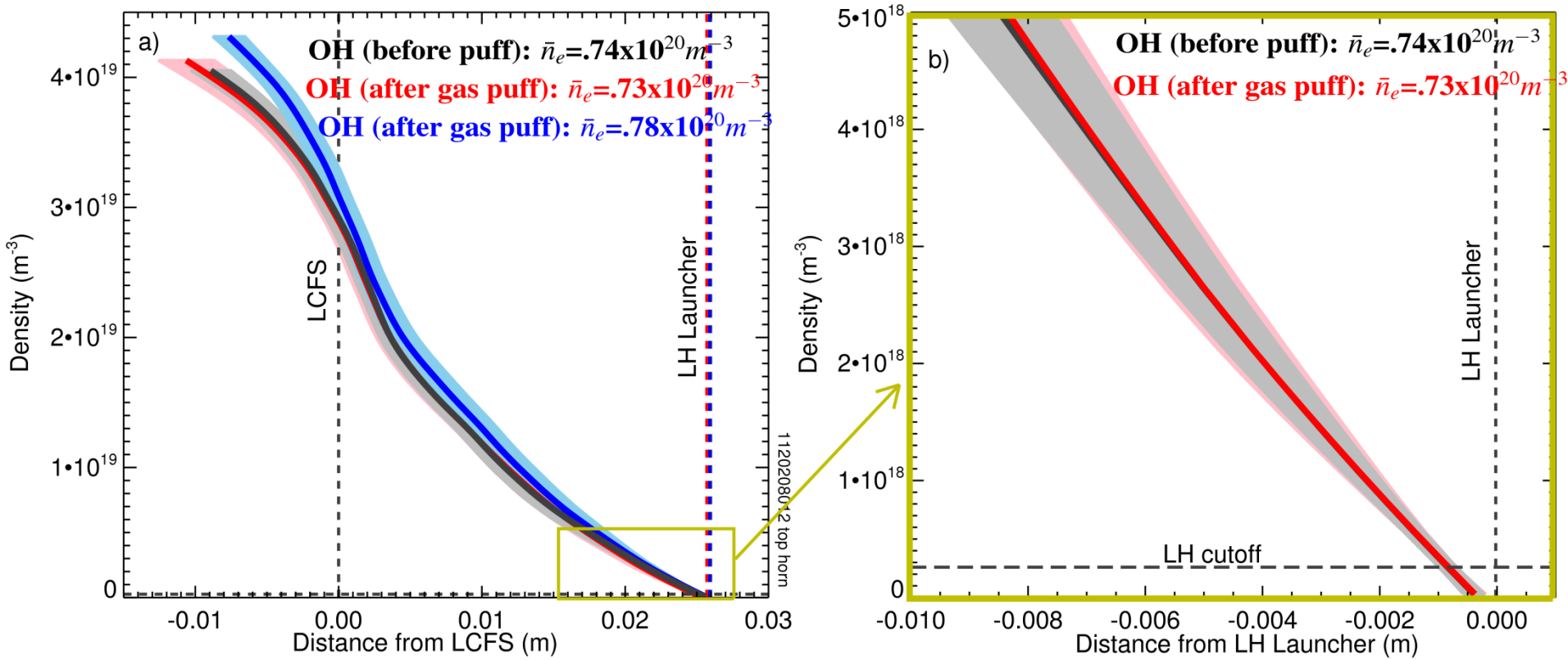

For high $\bar{n}_e > 1x10^{20}$ m^{-3} LH discharges, SOL density increases at middle horn *behind* LH launcher

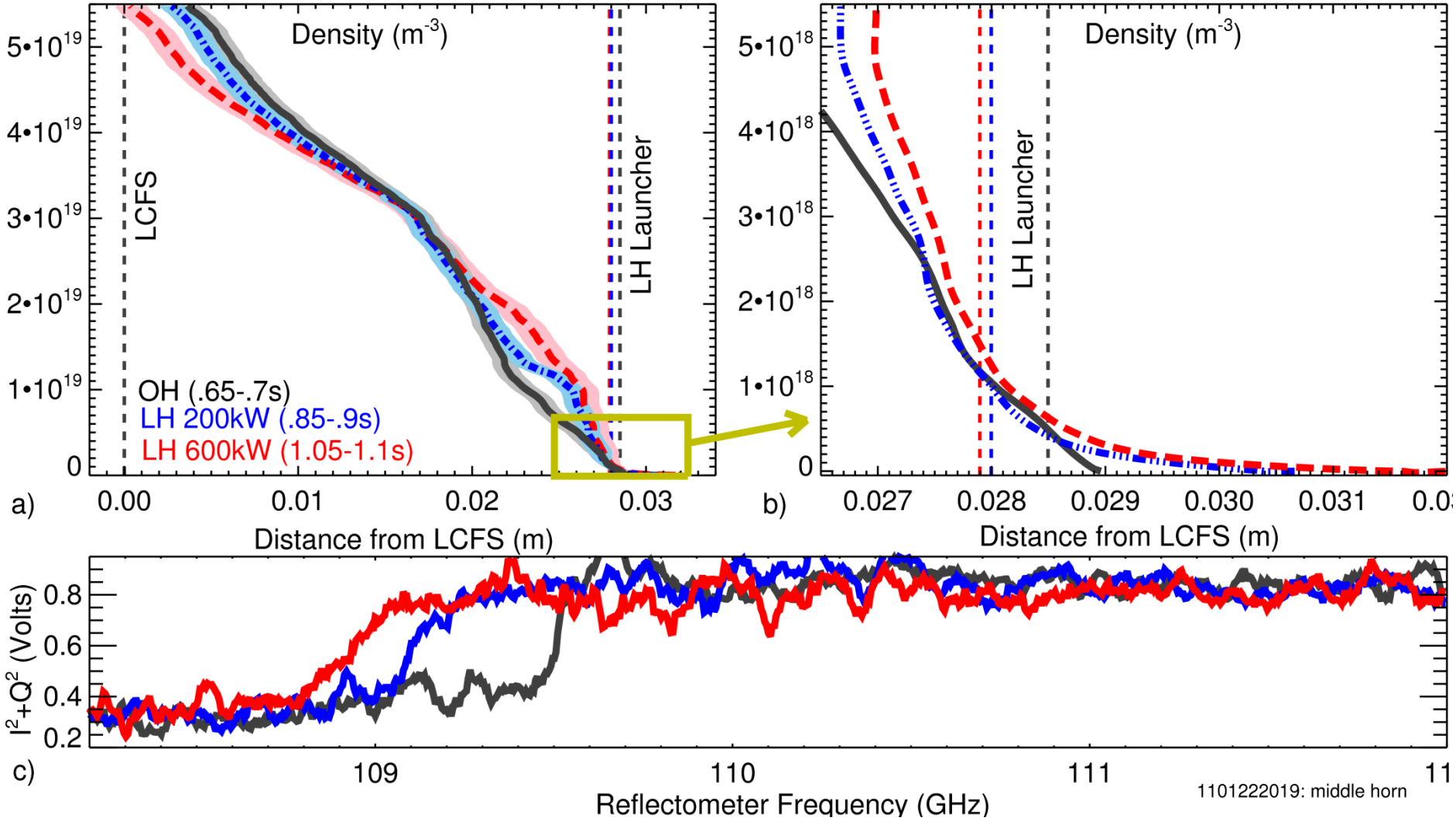

Density increase behind LH launcher only occurs for high $\bar{n}_e$ LH discharges at horn locations near striations

GPI can be used to measure radial profile of poloidal flows

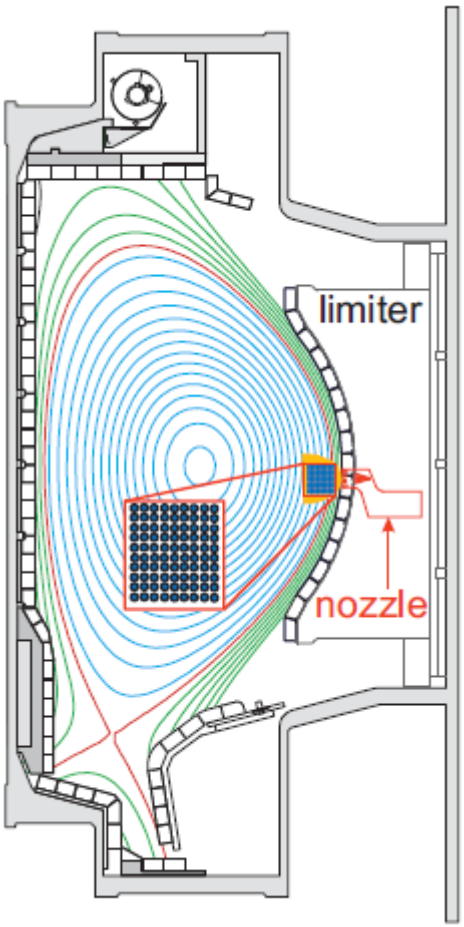

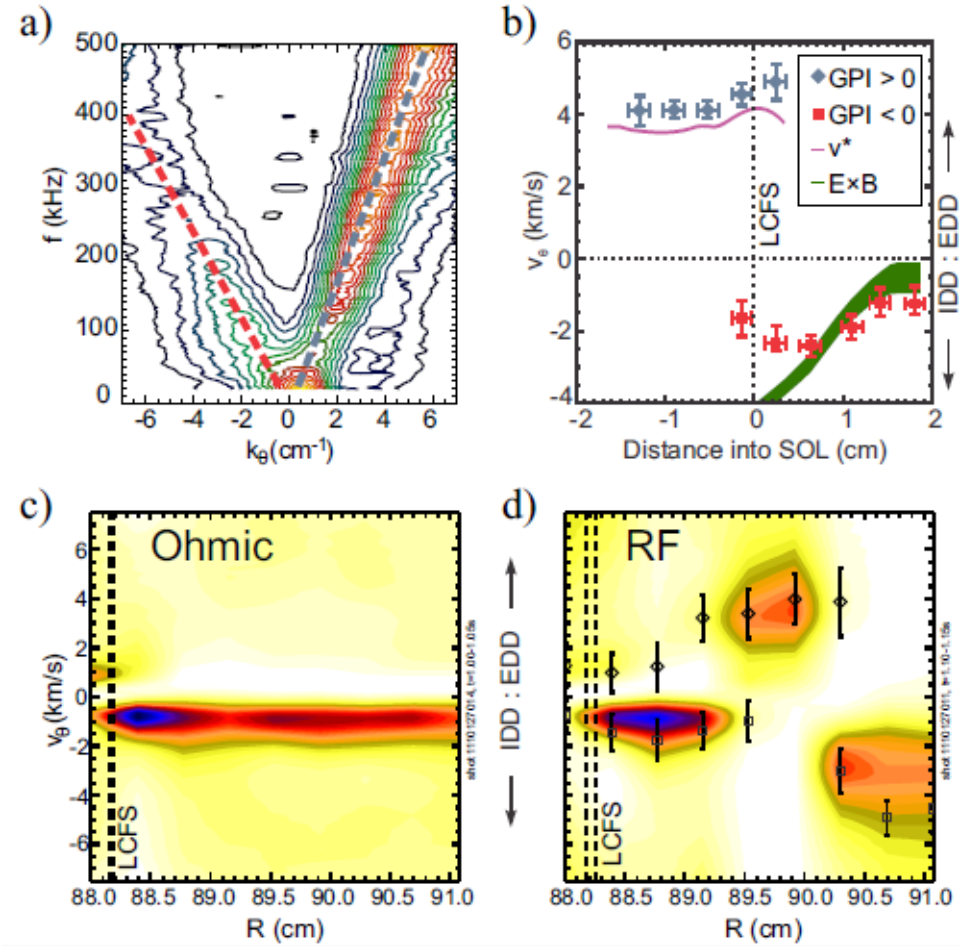

- poloidal and radial array that uses gas puff to localize He 586 nm line emission
- GPI is magnetically connected to LH launcher

- let poloidal phase velocity $(\omega/k_\theta) = v_{ExB}$
- above ansatz holds during OH discharges
- assume it is true for LH and ICRF discharges

Comparison between model and GPI data of ICRF-induced plasma potentials

typical flows during ICRF heated discharges

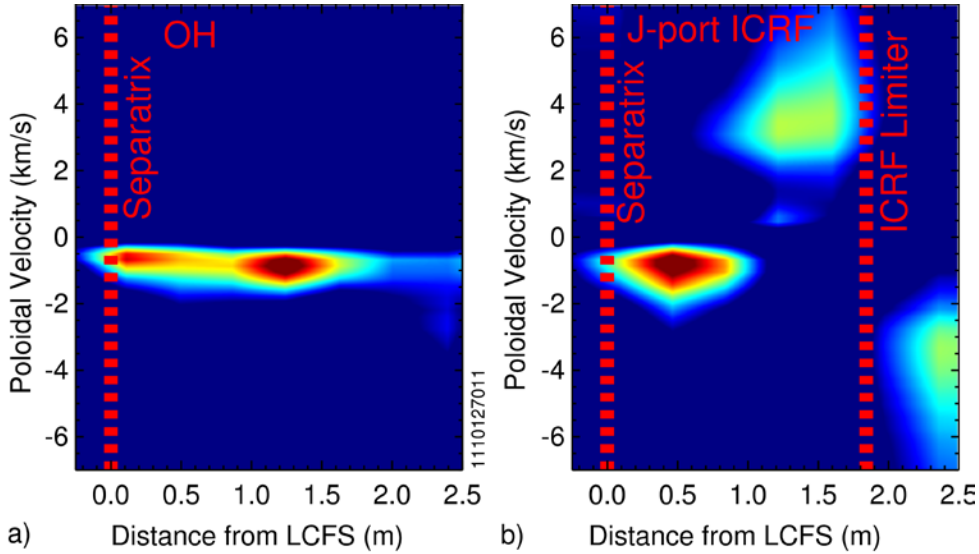

poloidal variation of plasma potential

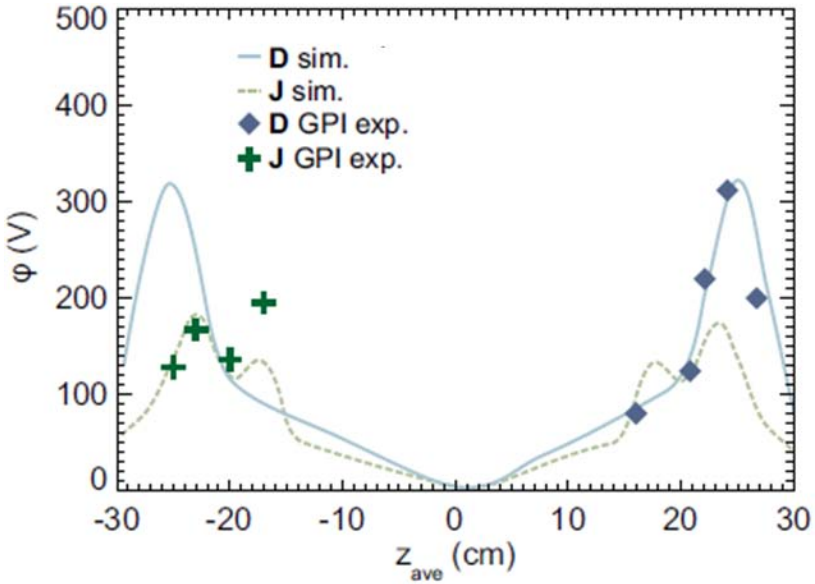

plasma potential with ICRF power

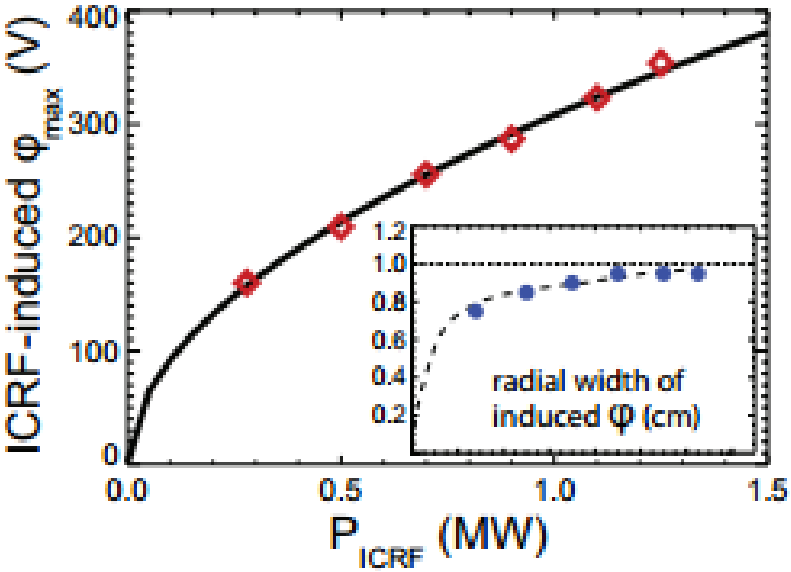

Comparison between field aligned ICRF and toroidally aligned ICRF antennas experimental measurement and simulation models do not agree

simulation difference between old J and new J

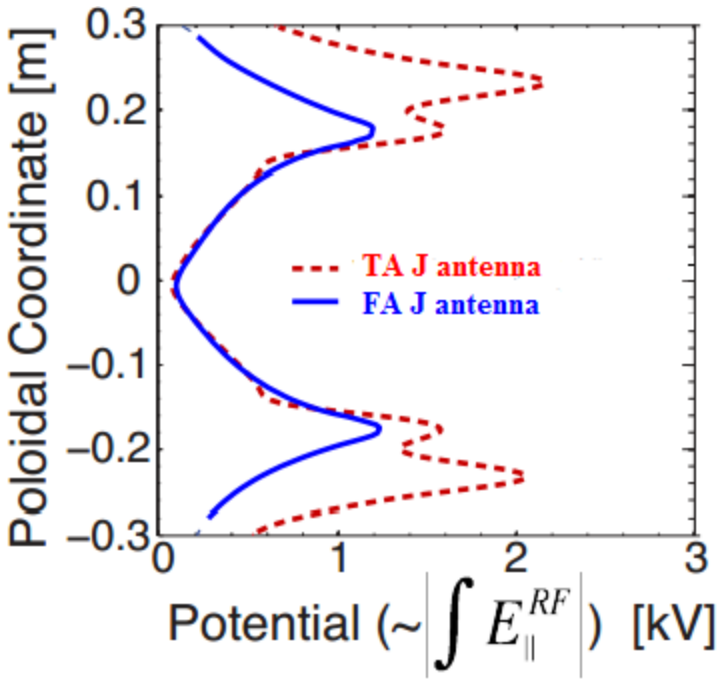

experimental difference between old J and new J

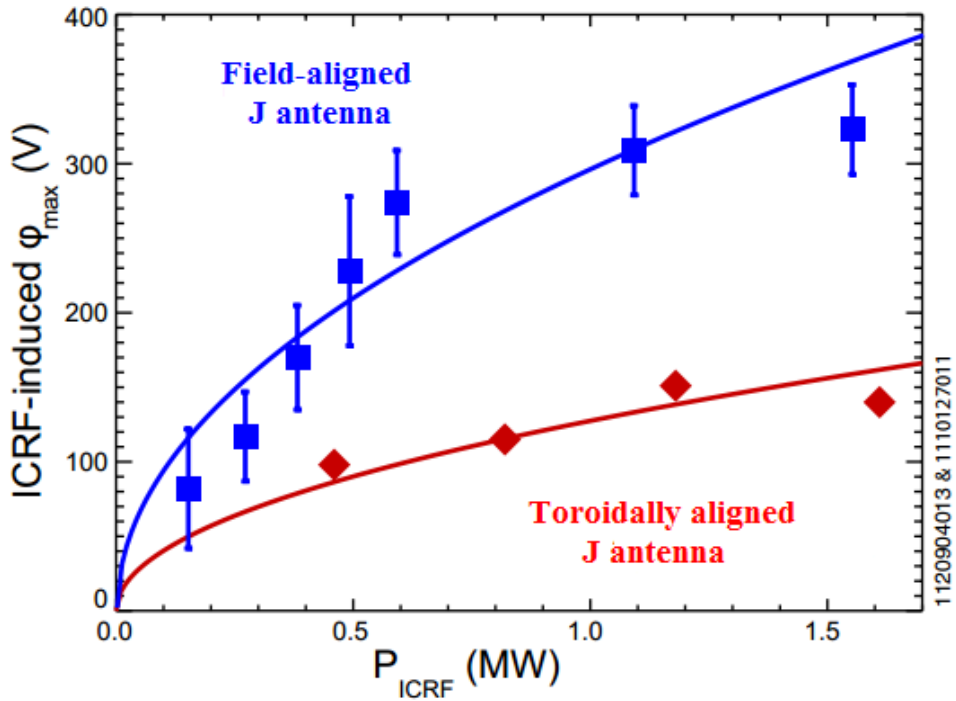

LH coupling efficiency during simultaneous LH+ICRF operation

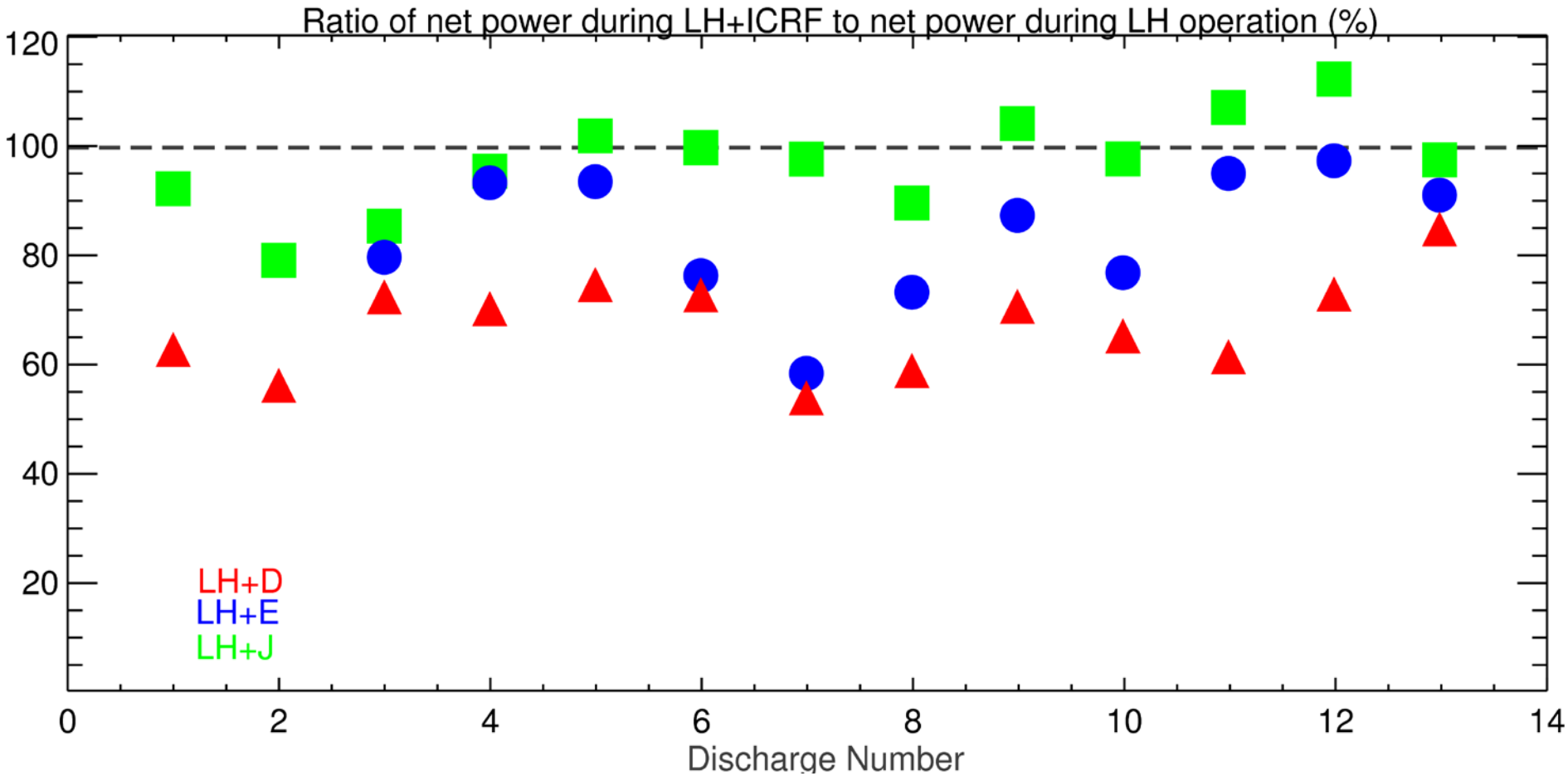

LH coupling is degraded for LH+D and LH+E operation for all discharges

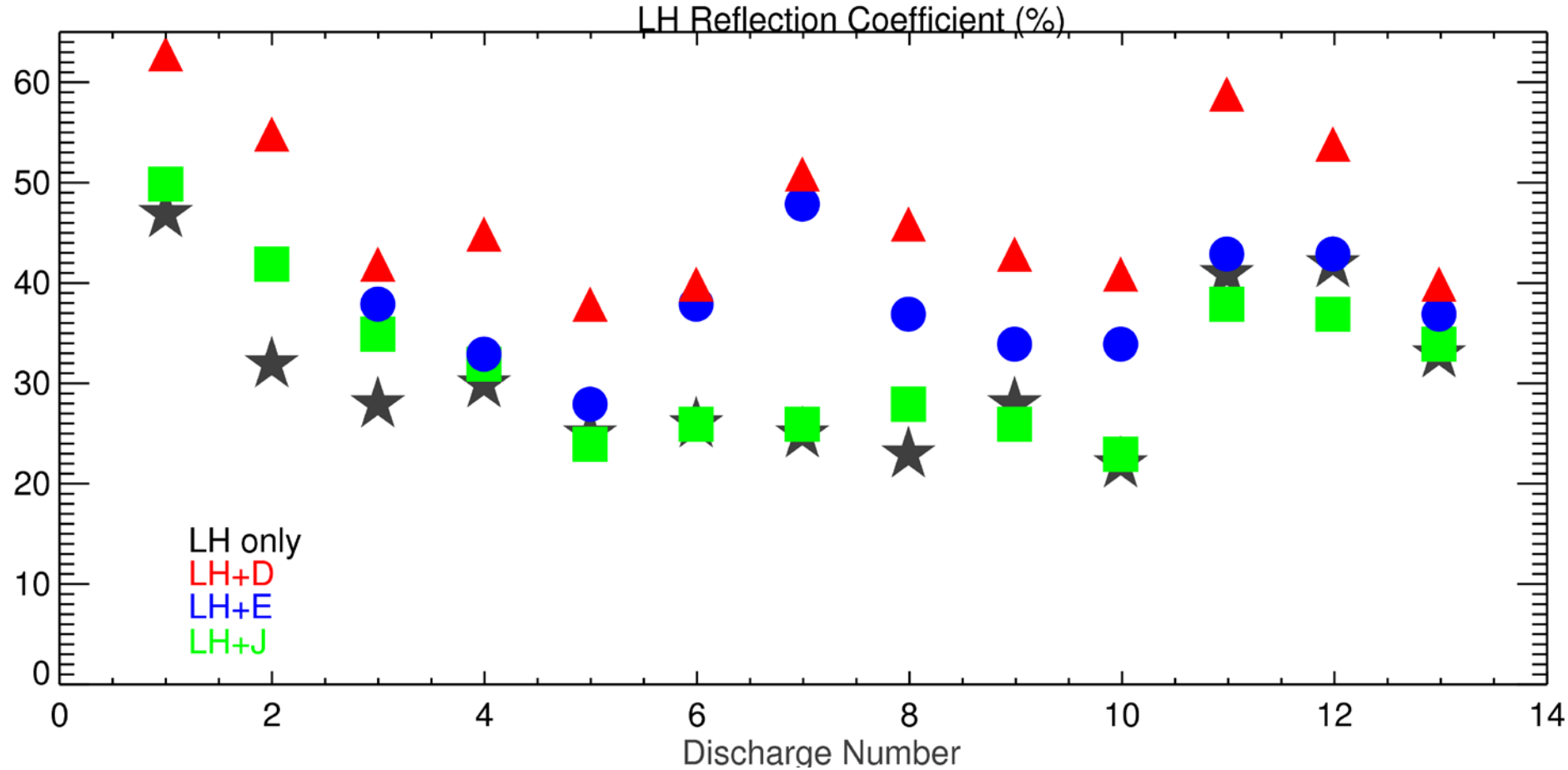

- reflection coefficient is minimally modified for LH+J, strongly modified for both LH+D and LH+E

- normalized net LH power relative to LH only operation is 70%, 80%, 95% with LH+D, LH+E, and LH+J

ICRF-induced density profile modifications

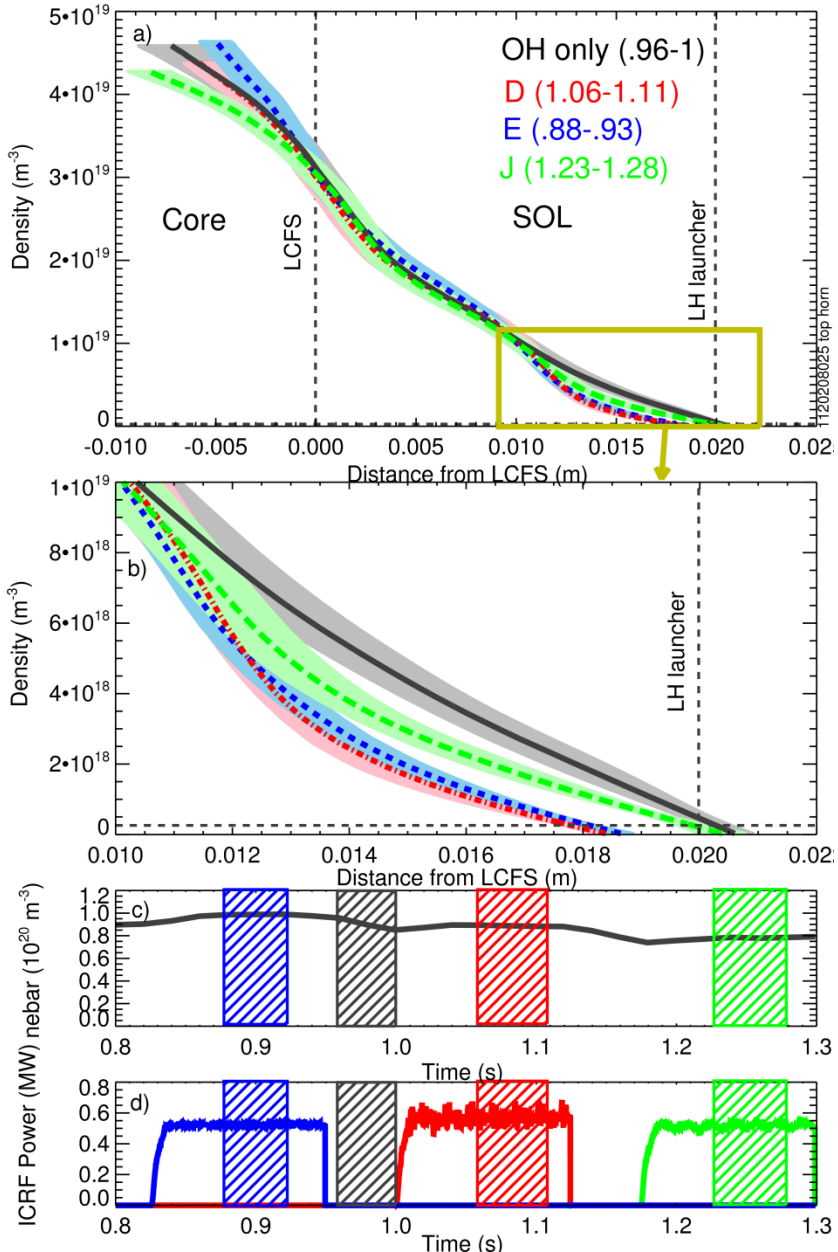

- reflectometer measurements show minimal change except for a few mm in front of LH launcher for all ICRF antenna configurations at all horn locations and for both toroidal magnetic field directions
- ICRF-induced density depletion is observed in front of LH launcher
- small density increase observed in near-SOL probably because of ICRF-induced outgassing
- not clear if this is consistent with models for ICRF sheaths

Table of results for dedicated LH+ICRF operation

#	$\bar{n}_e$	I_p	outer gap	LH location	ICRF order	LH	LH+D	LH+E	LH+J
1	.5-.7	.6	1.4	3	E-D-J	47	63	No data	50
2	.5-.7	.6	1.4	2	E-D-J	32	55	No data	42
3	.7-.8	.6	1.4	2	J-E-D	28	42	38	35
4	.7-.8	.6	1.4	2	J-D-E	30	45	33	32
5	1-1.1	.6	2	2	J-D-E	25	38	28	24
6	.8-.9	.6	1.9	1	J-D-E	26	40	38	26
7	.8-.9	.8	1.5	1	J-E-D	25	51	48	26
8	.8-.9	.8	1.2	1	J-E-D	23	46	37	28
9	.8-.9	.8	.9	1	E-D-J	28	43	34	26
10	.7-.9	1	.9	1	E-D-J	22	41	34	23
11	.7-.9	1	.6	4	E-D-J	41	59	43	38
12	.7-.9	.8	.6	4	E-D-J	42	54	43	37
13	1.-1.2	1	.6	4	E-D-J	33	50	37	34

Addition of LH power into ICRF EDA H-mode creates strong flows throughout edge and SOL plasma

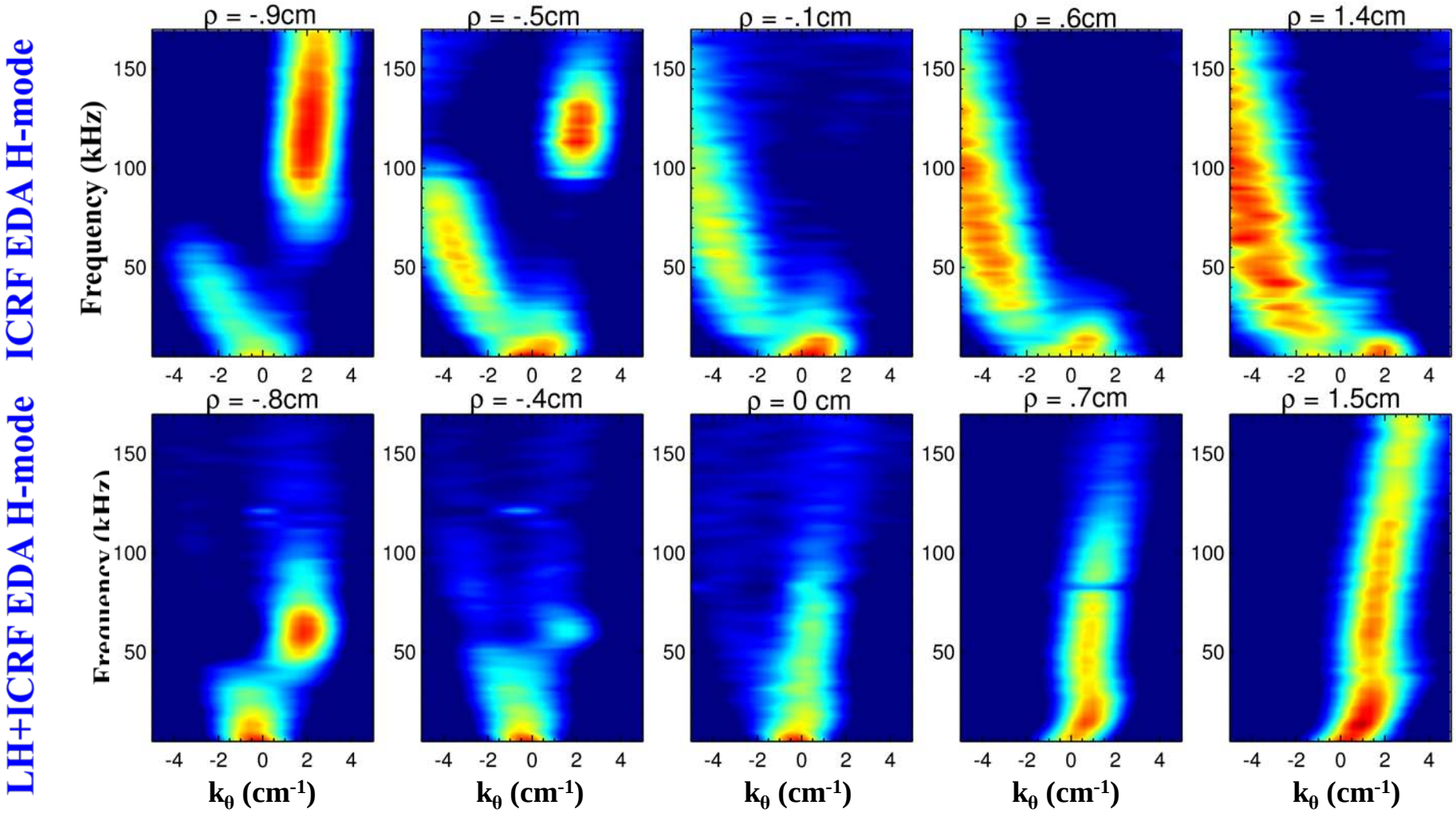

Addition of LH power leads to decrease in background fluctuation levels, density and temperature pedestal modifications, change in QCM frequency, enhancement in stored energy, **flow and flow shear in edge and SOL?**

Future work in understanding and improving ICRF/SOL, LH/SOL interactions in relationship to LH coupling

- better understanding of the complicated spatial structures of ICRF and LH-induced plasma flows and potentials
  - GPI measurements during inner gap, line averaged density etc. scans with LH will be extremely beneficial
    - preliminary measurements show strong LH-driven flows in edge and SOL during ICRF heated EDA H-modes
  - Simultaneous GPI and reflectometer measurements

- increased poloidal resolution of GPI, reflectometry

- direct measurement of LH and ICRF waves with reflectometry

- 3D diffusive-convective and LH coupling model that includes both radial and poloidal density profile asymmetries will provide predictive capability